Fabrication of optic and electromagnetic devices for experiments with ultra cold atoms

Dominik Fischer

1.April 2008

Abstract

The goal of this thesis was the development and fabrication of different devices for so-called atom chip experiments manipulating and detecting ultra cold atoms in the microkelvin regime. The first task was the design and construction of an imaging system for absorption imaging of ultra cold atoms trapped by the chip. The design of this lens system was done with the help of a ray tracing simulation program. The final system was characterized by taking pictures of test grating. With the help of Fourier analysis of these pictures the contrast in relation to the resolution was found. The limit of resolution was found at 10μm, which agreed with the simulated value. The second task was to use methods used in the micro-fabrication of integrated circuits, such as optical lithography, evaporation and sputtering metal films onto a substrate, to build devices for experiments with ultra cold atoms. At first the atom chip itself was built containing gold wires building electromagnetic traps and potentials for neutral atoms. These wires and therefore the potentials are built with a precision on the sub micrometer scale. For integrating a single atom fluorescence detector on the chip holding structures for the alignment of optical fibers are designed and built of SU-8. The final task was the construction of superconducting microwave resonators on the chip made of niobium.

Zusammenfassung

Das Ziel dieser Diplomarbeit war die Entwicklung und Fabrikation verschiedener Instrumente und Bauteile für sogenannte Atomchipexperimente, die ultrakalte Atome im Mikrokelvin-Regime manipulieren und detektieren. Die erste Entwicklung betraf das Design und die Konstruktion eines Imagingsystems für ein Absorptions-Imaging von ultrakalten vom Chip eingefangenen Atomen. Dieses Linsensystem wurde mithilfe eines optischen Raytracing-Programms entworfen. Mit dem endgültigen System wurden Bilder von einem Testgitter gemacht und mittels Fourieranalyse konnte der Kontrast in Abhängigkeit von der Auflösung dargestellt werden. Die ermittelte Auflösungsbegrenzung von 10μm stimmt mit dem simulierten Wert überein. Die zweite Aufgabe war das Verwenden von Methoden zur Herstellung integrierter Schaltkreise, wie optische Lithographie oder das Aufdampfen und Sputtern von Metallfilmen auf ein Substrat, für die Zwecke von Experimenten mit ultrakalten Atomen. Als erstes wurde der Atomchip selbst gebaut, welcher aus Golddrähten besteht, die elektromagnetische Fallen und Potentiale für neutrale Atome produzieren. Diese Drähte und damit die Potentiale werden mit einer Genaugkeit im Submikrometer-Bereich erzeugt. Für die Integration eines Floureszenzdetektors für einzelne Atome wurden Haltestrukturen aus SU-8 zur Ausrichtung von optischen Fasern geplant und gebaut. Als letztes wurde der Prozess zur Konstruktion von supraleitenden Mikrowellenresonatoren auf dem Chip aus Niob entwickelt.

Contents

Introduction **v**

I Theory 1

1 Fourier optics **2**
1.1 The Helmholtz Equation 2
1.2 The modulation transfer function 3
1.3 Propagation in free space 5
1.4 Fresnel approximation 5
1.5 Fraunhofer approximation 6
1.6 Diffraction 7
1.6.1 Diffraction limit of an optic system 7
1.6.2 Diffraction at a rectangular slit 7

2 Interaction of electromagnetic fields with atoms **8**
2.1 The choice of frequency 8
2.1.1 Static magnetic field: Zeeman shift 8
2.1.2 Near resonant waves 9
2.2 The choice of vacuum 10
2.2.1 Light: Induced Emission and Absorption 11
2.2.2 Vacuum: Spontaneous Emission 12
2.2.3 Cavity 13

II Fabrication and characterization 14

3 Absorption Imaging **15**
3.1 Design of the lens system 15
3.2 Fourier analysis of the test images 17
3.2.1 The sinc-function 17

3.2.2 Calibration of the resolved distances 18
3.2.3 Calculation of the modulation transfer function 19
3.2.4 The focal depth of the imaging system 21
3.3 Imaging atoms 22

4 Optical lithography for micro-fabrication 25

5 Fabrication of an atom chip 27
5.1 Design of an atom chip 27
5.2 Fabrication of a single layer atom chip 29
5.3 The chip trap 32

6 SU-8 holding structures for integrated micro-optics 35
6.1 SU-8 - A photoresist for high aspect ratio micro structures . . 35
6.2 Influencing the undercut of the structures 35
6.3 Lithographic processing with SU-8 50 40
6.4 A single atom fluorescence detector 41

7 Superconducting niobium microwave devices 43

Conclusion and outlook 46

Chip Recipes 48

Acknowledgements 54

Introduction

Technology and science are two very connected processes. New scientific breakthroughs lead to new technologies. But it may also occur that it is the other way around. This is the case, if well understood technologies are used in a new way or in a field of science completely different to which it is developed from in the first place. This kind of misuse takes place in the atom chip experiments. A nowadays well understood technology, namely the fabrication of integrated circuits on a chip, is used not to built devices for basic algebraic operations but it is used to manipulate ultra cold atoms near its surface. There are several reasons to do this. At first cold atoms produced by laser cooling can be treated quantum-mechanically. Thus it is possible to do experimental tests of quantum mechanics and atomic physics. First experiments for quantum information processing like storing quantum bits can be carried out. The second feature is related to the statistical mechanics of quantum gases in potentials, which are geometrically well-defined and therefore accessible for a closed mathematical description, or even gases in lower dimensions. The third process is the probable development of new technologies, not only on the byway, but also by implementing directly new methods to probe different properties of surfaces and electromagnetic or may be even gravitational fields.
This thesis can be seen as a step of an ongoing iteration process of using existent technologies, modifying it for experimental purposes, doing the experiment and apply its result for improvement or even change of the technological methods in use. In the course of this thesis there are gone several steps for different experiments therefore differing by the place in the iteration circle. But they all have in common that they take place at the technological side of the of it.
In principle four ideas are followed. At first the construction of an optic system to take images of light absorbed by atoms underneath the chip situated in a vacuum chamber. This task, creating a lens system being capable to image something with a proper resolution, has been carried out very often and is nothing new from a technological point of view. But to find an easy way

for the determination of its properties the method of Fourier optics is used, which can be easily implemented for data evaluation. Thus the improvement is to find more at the science side of the iteration circle.
The three other goals of this thesis are based on the technology of microfabrication integrated devices for experiments with ultra cold atoms. Their status in the iteration is differing from each other. There is first the fully understood technology of the fabrication process of a single layer atom chip, which became a kind of routine work in the atom chip group at the atomic institute Vienna where this thesis is carried out.
This is true as long as there are no further devices to build on the chip. One of these devices is an optical fluorescence detector integrated on the chip. This has been done once before with other geometrical properties, so this integration procedure of micro-optics on the chip has to be found. This would be a second loop step in the iteration because the changed properties came from the previous experiment.
Finally a completely new kind of experiment with ultra cold atoms is on its way to be carried out. This is the interconnection of atoms with superconducting solid state devices acting itself quantum mechanically. These two systems are coupled with the help of a superconducting microwave resonator. The fabrication of these resonator structures is tested for the first time in due this thesis. But it is not technology, which is new but only the experiment it is used for.
In summary the goal of this thesis is a test of different technologies for experiments with ultra cold atoms. But in the first place it is a motivation to learn about all these methods and to find an own access to it. A good painter has to be well-trained in the basic painting techniques before he can perform real art.

Part I

Theory

Chapter 1

Fourier optics

This chapter is an introduction to the optical properties discussed in this thesis based on Fourier analysis. Most of its content is following the references[1, 2], being two excellent sources for Fourier optics. For the discussion of optic systems, Fourier optics is an elegant tool. It is especially suitable for evaluation of pictures because functional methods of Fourier decompositions can easily be used for data analysis.

1.1 The Helmholtz Equation

The propagation of light is described by the wave equation

$$\left[\Delta - \frac{1}{c^2}\frac{\partial^2}{\partial t^2}\right] E(\vec{r},t) = 0, \tag{1.1}$$

where $E(\vec{r},t)$ is a scalar representation of the electromagnetic field, which holds as long as no anisotropic media are involved. Assuming monochromatic waves one can make a separation ansatz

$$E(\vec{r},t) = E(\vec{r})e^{-i\omega t} \tag{1.2}$$

and one obtains the Helmholtz-equation

$$\left[\Delta + k^2\right] E(\vec{r}) = 0 \tag{1.3}$$

by plugging the ansatz into the wave equation, where the wave vector $k = \sqrt{{k_x}^2 + {k_y}^2 + {k_z}^2} = \frac{\omega}{c}$ is introduced. For monochromatic waves propagating along the z-axis k_z can be expressed by the other two components

$$k_z = \sqrt{k^2 - k_x^2 - k_y^2} \tag{1.4}$$

The wave can be decomposed into a sum of spatial frequency components

$$E(\vec{r}) = \int E(k_x, k_y) e^{-iz\sqrt{1/\lambda^2 - k_x^2 - k_y^2}} e^{-i(k_x x + k_y y)} dxdy. \tag{1.5}$$

which can be inverted with the introduction of the entrance pupil function $E_0(x, y) := E(x, y, 0)$

$$E(k_x, k_y) = \int E_0(x, y) e^{i(k_x x + k_y y)} dxdy = F[E_0(x, y)] \tag{1.6}$$

Thus the electric field in k-space is the Fourier transform of the entrance pupil function. It is fully defined by the electric field at $z = 0$. For only the intensity $I = |E|^2$ is measurable the fact is used that convolutions in x-space can be decomposed into products in k-space

$$F[I(x, y)] = F[|E(x, y)|^2] = |F[E(x, y)]|^2 . \tag{1.7}$$

1.2 The modulation transfer function

For the characterization of optic systems two properties are important, namely contrast and resolution. These are related by the modulation transfer function (MTF) which is defined by

$$MTF(k) = \frac{I_{max}(k) - I_{min}(k)}{I_{max}(k) + I_{min}(k)}. \tag{1.8}$$

Thus the MTF relates the modulation of the measured intensity pattern to the spatial frequency. The smaller the distance to resolve the smaller is the contrast because the intensity pattern is washed out due to diffraction. Propagation through free space for example acts as a low pass filter in frequency space. To obtain the MTF for an optic system the measured intensity pattern $I(x, y)$ has to be related to the intensity $I_0(x, y)$ at the entrance pupil. Thus the electric field E is written as a functional of E_0

$$E = E[E_0(x, y)]. \tag{1.9}$$

One can do a functional Taylor expansion of $E[E_0(x, y)]$ around $E_0(x, y) = 0$

$$E[E_0(x, y)] = E[E_0(x, y)]\big|_{E_0=0} + \int \frac{\delta E[E_0(x, y)]}{\delta E_0(x', y')}\Big|_{E_0=0} E_0(x', y')dx'dy' + \dots \tag{1.10}$$

Optic systems can be treated in the far field regime where the output field is related to the input field by a linear operation. Therefore higher order terms can be neglected and the relation for the wave can be written as

$$E[E_0(x,y)] = \int \frac{\delta E[E_0(x,y)]}{\delta E_0(x',y')}\Big|_{E_0=0} E_0(x',y')dx'dy', \tag{1.11}$$

because the resulting field vanishes if the input intensity is zero. The physical meaning of the functional derivative is easily obtained if $E_0(x,y) = \delta(x-x')\delta(y-y')$ is set for the field, defining a point-like source,

$$\begin{aligned} E[E_0(x,y)] &= \int \frac{\delta E[E_0(x,y)]}{\delta E_0(x',y')}\Big|_{E_0=0} \delta(x-x')\delta(y-y')dx'dy' && (1.12)\\ &= \frac{\delta E[E_0(x,y)]}{\delta E_0(x',y')}\Big|_{E_0=0} = S(x,y,x',y') && (1.13) \end{aligned}$$

Thus the derivative explains, how a single point is washed out by the optic system, and $S(x,y)$ is therefore called point spread function (PSF). The Fourier transform of the PSF is the transfer function

$$H(k_x,k_y) = F[PSF] = \int S(x,y)e^{i(k_x x + k_y y)}dxdy, \tag{1.14}$$

because it is the sum over all elementary waves produced by a light source built of an infinitesimal sum of point sources. For the intensity of the system the absolute square can be built

$$I(k_x,k_y) = |H[k_x,k_y)]|^2 I_0(k_x,k_y) \tag{1.15}$$

This value is the modulation transfer function $MTF = |H|^2$.

1.3 Propagation in free space

Propagation through free space can be described by

$$E(x', y') = E_0(x, y)e^{i(k_z d)}, \tag{1.16}$$

Thus we obtain for the transfer function in free space

$$H(k_x, k_y) = e^{id\sqrt{k^2 - k_x^2 - k_y^2}}. \tag{1.17}$$

If $k_x^2 + k_y^2 > 1/\lambda$, the wave is attenuated by 1/e at a distance of

$$d_{1/e} = \frac{1}{\sqrt{k_x^2 + k_y^2 - k^2}} \tag{1.18}$$

This leads to a low pass behavior of free space with a spatial cut-off frequency $1/\lambda$. Thus if the propagation distance is smaller than $d_{1/e}$, resolution is not limited in principle because the transfer function only produces a phase shift. This is applied in contact lithography, where the miniaturization of the resolvable structures is only limited by the production process of lithography masks and the optical properties of the irradiated material.

1.4 Fresnel approximation

The argument of the transfer function can be approximated by

$$d\sqrt{k^2 - k_x^2 - k_y^2} = kd\sqrt{1 - \frac{k_x^2 - k_y^2}{k^2}} \approx kd(1 - \frac{k_x^2 - k_y^2}{2k^2}) \tag{1.19}$$

This Fresnel-approximation is valid if the quadratic term is negligible, which means that only paraxial waves are regarded. The field at $z = d$ reads

$$\begin{aligned} E(x, y) &= F[E(k_x, k_y)H(k_x, k_y)] & (1.20)\\ &= e^{-ikd} \int E_0(k_x, k_y)e^{i\frac{d}{2k}(k_x^2 + k_y^2)} \frac{e^{-i(k_x x + k_y y)}}{2\pi} dk_x dk_y & (1.21) \end{aligned}$$

The point spread function for propagation in free space is the inverse Fourier transform of the transfer function

$$S(x, y) = F^{-1}[H(k_x, k_y)] = \frac{ike^{-ikd}}{d} e^{i\frac{k}{2d}(x^2 + y^2)} \tag{1.22}$$

With this the propagation in space can be calculated

$$E[E_0](x,y) = \frac{ike^{-ikd}}{d} \int E_0(x',y') e^{-i\frac{k}{2d}((x-x')^2+(y-y')^2)} dx'dy' \tag{1.23}$$

1.5 Fraunhofer approximation

By going much further away from a light source than the width of it the Fraunhofer approximation can be applied to the argument of the point spread function

$$\frac{k}{2d}(x'^2 + y'^2) << 1, \tag{1.24}$$

which leads to

$$E[E_0](x,y) = \frac{ike^{-ikd}}{d} e^{-i\frac{k}{2d}(x^2+y^2)} \int I_0(x',y') e^{i\frac{k}{d}(xx'+yy')} dx'dy' \tag{1.25}$$

By introducing

$$k_x := \frac{kx}{d},\ k_y := \frac{ky}{d} \tag{1.26}$$

it is found that the output signal

$$E[E_0(x,y)] = S_0 E_0(k_x, k_y) \tag{1.27}$$

is proportional to the Fourier transform of the input signal if one restricts to the output region near the axis. This means that in the far field regime the Fourier transform of the entrance pupil is observed. This is called optical Fourier transform and can be corrected by installing a lens system acting itself as a Fourier transformer. Thus lens systems can correct diffraction up to their own diffraction limit.

1.6 Diffraction

Optic system are always spatially limited which naturally leads to diffraction at these limiting pupils.

1.6.1 Diffraction limit of an optic system

One of the most important values for lens systems is the limit of resolution due to diffraction. This can be calculated by applying the Fraunhofer limit

$$I[I_0] = \frac{I_0}{(\lambda d)^2}|F[E_0(\frac{x}{\lambda d}, \frac{y}{\lambda d})]|^2 \tag{1.28}$$

where the intensity is calculated taking the lens on the image side as pupil with diamater D

$$I(x,y) = (\frac{kD^2}{2d})^2 \left[\frac{J_1(kDr/2d)}{kDr/2d}\right]^2, \tag{1.29}$$

where $r = \sqrt{x^2+y^2}$. Thus the limit of resolution is given at the first minimum of the Bessel-function J_1 with the Airy-radius

$$r = 1.22\frac{\lambda d}{D} \tag{1.30}$$

this corresponds to Rayleighs criterion if the focal length of the system is set for d.

1.6.2 Diffraction at a rectangular slit

For the rectangular problem in the Fraunhofer approximation a similar expression to 1.29 can be found

$$I(x,y) = (\frac{kD_xD_y}{2d})^2 sinc^2(kD_xx/2d)sinc^2(kD_yy/2d), \tag{1.31}$$

with the introduction of the sinc-function defined by $\frac{\sin x}{x}$.

Chapter 2

Interaction of electromagnetic fields with atoms

In order to be able to do experiments with atoms one has to understand the interaction between electromagnetic fields and atoms. This is important not only because every measurable physical property is translated into an electronic signal in the end for evaluation but electromagnetic fields are the main tools to control and manipulate atoms. This introduction follows mostly [3] and the part about cavities is described in [4].

2.1 The choice of frequency

Talking about the interaction between electromagnetic fields and atoms one has to restrict to a certain field configuration.

2.1.1 Static magnetic field: Zeeman shift

For trapping atoms on the chip one has to investigate its behavior in a static magnetic field. We have to consider at first the level structure due to the hyperfine splitting. The coupling between the total angular momentum of the electron **J** and the nuclear spin **I** leads to the introduction of a conserved total angular momentum of the atom

$$\mathbf{F} = \mathbf{J} + \mathbf{I}. \tag{2.1}$$

The level splitting due to this summation of angular momenta is given by the eigenvalues of the interaction Hamiltonian

$$\hat{H}_F = A\mathbf{J} \cdot \mathbf{I} \tag{2.2}$$

which are calculated by going to the eigenbasis of the "good" quantum number **F**

$$|IJm_Im_J\rangle = \sum_{m_F} \langle Fm_F|IJm_Im_J\rangle \, |Fm_F\rangle \, . \tag{2.3}$$

These eigenvalues can be expressed by

$$E_{HF} = \frac{A}{2}(F(F+1) - J(J+1) - I(I+1)). \tag{2.4}$$

Then the coupling of of the magnetic momentum produced by **F** to an external magnetic field **B** has to be investigated. This Zeeman effect is described by the Hamiltonian

$$\hat{H} = g_F \mu_B \mathbf{F} \cdot \mathbf{B}, \tag{2.5}$$

with the resulting Landé factor

$$g_L = \frac{F(F+1) - J(J+1) - I(I+1)}{2F(F+1)} g_J. \tag{2.6}$$

From this point on the atom is treated like a two-level system throughout this chapter, which is put into different environments corresponding to the regarded experimental situation. By the choice of the right two-level system a magnetic trap can be built. From the optical Earnshaw theorem follows, that static magnetic field maxima do not exist in free space. Therefor the atoms have to be trapped in a so-called low field seeking state, where their magnetic moment looks in the opposite direction of the field. Then they are trapped in a field minium, where the energy is minimal.

2.1.2 Near resonant waves

For a monochromatic wave, which is on resonance with the atomic transition, the interaction is described by a time dependent potential in the Hamiltonian. The leading interaction between the field and the atom is the coupling of the electric field to the atomic dipole moment

$$\hat{V}(t) = \mathbf{d} \cdot \mathbf{E}(t). \tag{2.7}$$

By treating the wave classically and by choosing the polarization in the x-direction a scalar expression for 2.7 is found

$$\hat{V}(t) = \frac{e\hat{x}E_0}{2}(e^{i\omega t} + e^{-i\omega t}). \tag{2.8}$$

The time evolution of the two-level system

$$|\Psi\rangle = c_g(t)e^{\frac{i}{\hbar}E_0 t}|g\rangle + c_e(t)e^{\frac{i}{\hbar}E_1 t}|e\rangle \tag{2.9}$$

has to be taken into account because of the time dependent potential. The coefficients c_g and c_e define the populations of the two states. By applying the the full Hamiltonian on the state 2.9 and projection onto the two solutions of the time independent Schrödinger equation a set of two coupled differential equations for these coefficients

$$\dot{c}_g(t) = -\frac{i}{\hbar}(c_g(t)V_{gg} + c_e(t)V_{ge}e^{-i\omega_0 t}) \tag{2.10}$$

$$\dot{c}_e(t) = -\frac{i}{\hbar}(c_g(t)V_{eg}e^{i\omega_0 t} + c_e(t)V_{ee}) \tag{2.11}$$

is found, with the atomic transition frequency $\omega_0 := \frac{E_e - E_g}{\hbar}$ and the matrix elements $V_{ij} = \langle i|\hat{V}|j\rangle$ in the basis of the time independent states. By inserting the potential into this relation

$$V_{ij}(t) = -\frac{E_0}{2}(e^{i\omega t} + e^{-i\omega t})\langle i|\hat{d}|j\rangle \tag{2.12}$$

and the definition of the Rabi frequency

$$\Omega_R = \frac{d_{eg}E_0}{\hbar} \tag{2.13}$$

we obtain

$$\dot{c}_g(t) = \frac{i}{2}\Omega_R(e^{i(\omega-\omega_0)t} + e^{-i(\omega+\omega_0 t)})c_e(t) \tag{2.14}$$

$$\dot{c}_e(t) = \frac{i}{2}\Omega_R(e^{-i(\omega-\omega_0)t} + e^{i(\omega+\omega_0 t)})c_g(t) \tag{2.15}$$

for this system. These equations describe the behavior of the two level system in a classical electromagnetic wave.

2.2 The choice of vacuum

Radiative transitions of the two level system were first investigated by Einstein, who had to introduce the concept of induced emission and absorption to obtain Planck's law in the state of thermal equilibrium between atoms and light[9].

2.2.1 Light: Induced Emission and Absorption

Following the steps of the previous chapter, where the atom is put into an environment of a classical electromagnetic wave, a solution to 2.14 has to be found. A typical initial condition is to prepare the atom in the ground state

$$c_g(0) = 1,\ c_e(0) = 0. \tag{2.16}$$

By assuming a low intensity the ground state can be seen fully populated $\dot{c}_g(t) = 0$ approximately for all times, which leads to

$$\dot{c}_g(t) = 0 \tag{2.17}$$

$$\dot{c}_e(t) = \frac{i}{2}\Omega_R(e^{-i\Delta t} + e^{i(\omega+\omega_0 t)}), \tag{2.18}$$

where $\Delta = \omega - \omega_0$ is the detuning from resonance. The solution of 2.17 is

$$c_g(t) = 1 \tag{2.19}$$

$$c_e(t) = \frac{i}{2}\Omega_R(\frac{e^{-i\Delta t} - 1}{-i\Delta} + \frac{e^{i(\omega+\omega_0)t)} - 1}{i(\omega + \omega_0)}) \tag{2.20}$$

If the rotating wave approximation is applied which holds for the near resonant case $\Delta << \omega + \omega_0$, the fast oscillating term are small and it is found

$$|c_e|^2 = (\frac{\Omega_R t}{2})^2 sinc^2(\frac{\Delta t}{2}) \tag{2.21}$$

for the population of the exited state. In order to obtain a physical correct result, a certain spectral width γ has to be assumed for the wave

$$E_0^2 = \frac{2}{\epsilon_0}\int_{\omega_0+\gamma/2}^{\omega_0+\gamma/2} u(\omega)d\omega. \tag{2.22}$$

This leads to

$$|c_e|^2 = \frac{d_{ge}^2 t^2}{2\epsilon_0\hbar^2}\int u(\omega)sinc^2(\frac{\Delta t}{2})d\omega \tag{2.23}$$

$$= \frac{d_{ge}^2 \pi t}{\epsilon_0\hbar^2}u(\omega_0), \tag{2.24}$$

where a perfect monochromatic wave is reintroduced. By comparing 2.23 with the Einstein-relation

$$\frac{dN_e}{dt} = B_{ge}^{\omega} u(\omega_0) N_g \tag{2.25}$$

it is found

$$B_{ge}^{\omega} = \frac{d_{ge}^2 \pi}{3\epsilon_0 \hbar^2}. \tag{2.26}$$

2.2.2 Vacuum: Spontaneous Emission

Putting an atom into real vacuum leaves only the interaction with the electromagnetic vacuum fluctuations. The vacuum energy of the electromagnetic field can be written as

$$E_{vac} = \frac{\hbar\omega}{2} = \int \frac{1}{2}(E \cdot D + H \cdot B) dV = \frac{E^2 V_0}{\epsilon_0}, \tag{2.27}$$

where a constant density of vacuum fluctuations is assumed in the the volume V_0 This leads to

$$E = \sqrt{\frac{\hbar\omega}{2\epsilon_0 V_0}} \tag{2.28}$$

The lifetime of the dressed state $|e, 0\rangle$ is the inverse of the transition rate, which is obtained by Fermi's golden rule

$$\Gamma_{eg} = 1/\tau = \frac{2\pi}{\hbar} |M_{eg}|^2 g(\omega). \tag{2.29}$$

with the density of states $g(\omega) = \omega^2/\pi^2 c^3$ and the matrix element$|M_{eg}|$ of the atomic transition

$$M_{eg}^2 = \frac{d_{eg}^2 E^2}{3} = \frac{d_{eg}^2 \hbar\omega}{6\epsilon_0 V_0} \tag{2.30}$$

which has to be averaged over all polarizations. This gives for the transition rate

$$\Gamma_{eg} = \frac{d_{eg}^2 \omega^3}{3\hbar\pi\epsilon_0 V_0}. \tag{2.31}$$

By comparing this to the Einstein-relation for spontaneous emission

$$\frac{dN_e}{dt} = -A_{ge} N_e \tag{2.32}$$

it is found that

$$A_{ge} = \Gamma_{eg}. \tag{2.33}$$

2.2.3 Cavity

Another form of vacuum is found inside a cavity. This changes the number of modes into which the atom can emit a photon. It enhances emission, if the cavity is built near resonance of the two-level transition and it suppresses it in the off-resonant case. Spontaneous emission can be described by the Purcell factor

$$F_P = \frac{\tau}{\tau_c} \tag{2.34}$$

which is quotient of the lifetime τ of the state $|e, 0\rangle$ in free space and the lifetime in the cavity τ_c. The main difference between these two cases is the density of states, which has a Lorentzian profile around the resonance frequency of the cavity. At resonance the Purcell factor reduces to

$$F_P = \frac{3Q(\lambda/n)^3}{4\pi^2 V_0}, \tag{2.35}$$

where the quality $Q = \omega_c/\gamma_c$ of the cavity is introduced. A combined energy level system for the dressed state can be described by the Jaynes-Cummings model. The energy is split

$$E_\pm = \hbar\frac{\omega_c + \omega}{2} \pm \hbar\sqrt{\Omega_R^2 + \Delta^2} \tag{2.36}$$

in the dressed state space, due to coupling of the electromagnetic mode ω_c in the cavity with the two-level system with the coupling strength described by the Rabi frequency and with the detuning Δ between both systems. This splitting also occurs, if the atom is put into an empty cavity, due to the existence of the cavity vacuum energy. This splitting can be observed in the strong coupling regime, where the coupling is much stronger then the photon loss rate. This leads to a cyclic decay of the atom into the cavity mode and reabsorption of it. This coupling of an atom or another sold-state two-level system to a microwave cavity is used for the quantum interconnect project. There the strong coupling is reached by high quality factors of a superconducting resonator in a low temperature environment.

Part II

Fabrication and characterization

Chapter 3

Absorption Imaging

For the detection of atoms in the MOT they have to be imaged. One way of imaging atoms is to look at their absorption profile. In due this thesis such an absorption imaging was designed.

3.1 Design of the lens system

The lens system for the absorption imaging was designed using a ray tracing simulation program[1]. Several configurations with lenses available on the market were tested for the given geometrical properties of the vacuum chamber. A combination of two so-called achromats were chosen to be a suitable configuration. Achromats are made of a biconvex and a biconcave lens made of differing glass types. This combination minimizes spherical abberation and coma and achieves magnification only due to the difference in the refractive index of the glass. The first achromat with a focal length of 175mm collimates the diverging rays of the atom cloud and the second one with f=300mm focuses them onto the surface of the CCD[2] chip. The final design is illustrated in figure 3.1.

The simulation traces the rays of spots on the object side of the lens system to its image side. The imaged spot as a function of the location of the spot on the object side is called Point Spread Function (PSF). The distances between the optical devices were varied by the simulation program in order to optimize the system due to the spot size at the image. At first the foci of the two achromats were found by tracing parallel rays through them separately. For the f=175mm lens the glass window of the vacuum chamber located 81mm away from the center of the atom chip had to be

[1]The used program was Zemax

[2]Charge Coupled Device

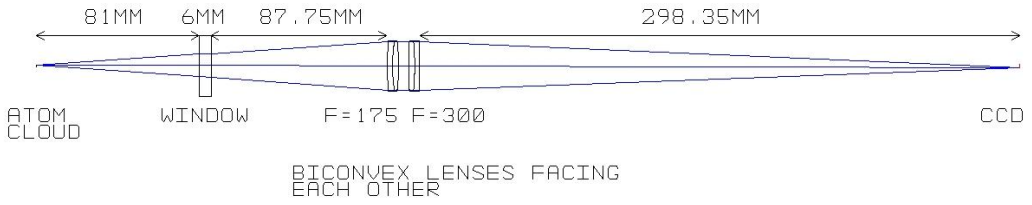

Figure 3.1: Design of the imaging system by the use of Zemax

considered. It was tested if the rays in between the two achromats would be parallel by optimizing the focus for large distances between the lenses. Even for distances of the order of hundreds of meters the optimal focal length did not change more than of the order of micrometers. The final values of the distances between the different surfaces, the radii of their curvature and the glass types is listed in table 3.1.

Surface	Curvature[mm]	Thickness[mm]	Glass
CENTER OF CHIP	∞	81,000000	
WINDOW	∞	6,000000	BK7
	∞	87,755726	
F=175 ACHROMAT	286,880000	2,500000	N-SF5
BICONCAVE	81,886000	3,000000	N-BK7
BICONVEX	-100,668000	5,000000	
F=300 ACHROMAT	187,461000	3,000000	N-BK7
BICONVEX	-134,005000	2,500000	N-SF5
BICONCAVE	-385,149000	298,353880	
CCD CHIP	∞	0,000000	

Table 3.1: Table of the different surfaces of the optical system and their distances to the next surface. The curvature radius may be given due to fact that only spherical lenses and flat surfaces are in use. The different glass types are BK7 and SF5, where the N stands for lead free glass. The fields left out are vacuum respectively air. These values are calculated using Zemax

The simulated spot sizes on the image plane had a root mean square radius of about 3μm near the optical axis and were still smaller than the

diffraction limit going away up to 2mm off-axis.

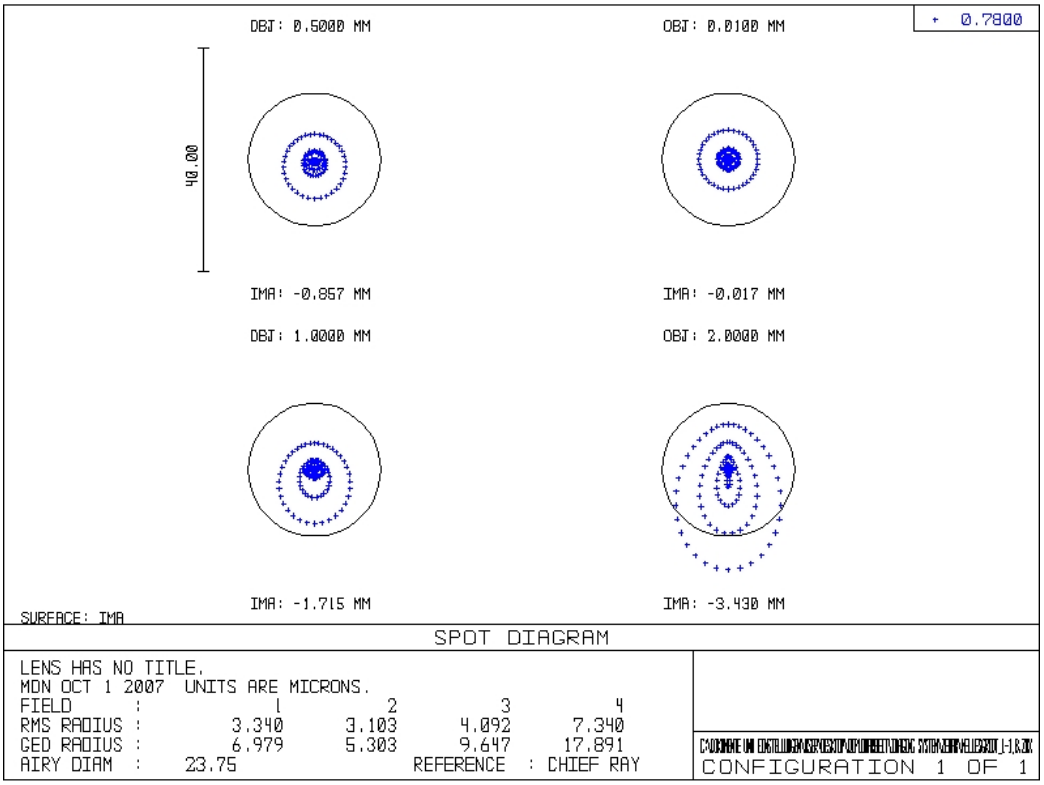

Figure 3.2: Simulated spot sizes for rays differing by their distance to the optic axis. The optic system is diffraction limited going up to 2mm off-axis, because the spot are inside the Airy disc defining the diffraction limit due to Rayleigh criterion. The values from the simulation have to be divided by the magnification of the system.

3.2 Fourier analysis of the test images

3.2.1 The sinc-function

The modulation transfer function, which relates the contrast to the resolved spatial frequency, is obtained by discussion of the Fourier components of an image. To determine the optic properties of the imaging system, pictures of a test grating with a varying number of lines per millimeter are taken. Due to the line structure of the test grating one can restrict this discussion to Fourier transformed lines of pixels perpendicular to the grating. An ideal

imaging system would produce a perfect rectangular intensity profile with vanishing intensity at the location of the lines of the grating and with the full intensity of the used light source at the locations between the lines. The one-dimensional Fourier transform of the ideal signal is the sinc-function

$$f(x) = rect(ax) \rightarrow F[f(x)] = \frac{\sin(2\pi ka)}{\pi k}, \tag{3.1}$$

where $2a$ is the width of one step of the rectangular function and k is the spatial frequency. For the discussion of real images the intensity profiles are Fourier transformed and the mean value over each transformed line of the picture is taken. This mean value is compared to the sinc-function of an ideal signal, which has to be understood in order to get an approach to the optical properties of the imaging system. The local extrema of the sinc-function at $k = n/a$, with n odd, are the amplitudes of the nth harmonics of the Fourier expansion. The height of the maximum at $k = 0$ is the intensity of the background around which the signal modulates, the first harmonic is determines the amplitude of the signal itself and the other maxima are the higher order harmonics of the Fourier expansion of the rectangular function. Every deviation of the sinc-function is due to certain imperfections of the optical system, such as defocus or interference.

3.2.2 Calibration of the resolved distances

The fast Fourier transform of the optical signal has one degree of freedom due to the scaling of the number of pixels per unit length. Using the images of the grating in combination with the knowledge of the exact number of lines per millimeter one can easily identify the location of the maxima in frequency space with a certain spatial frequency. This is done with images from 5 to 75 lines per millimeter. The unit of the k-axis of the spectrum derived by Fourier transformation is $1/Pixel$ and it is therefore related to the number of pixels per millimeter. The pixel size of the used CCD chip is $6.45\times6.45\mu$m which leads to a number of 155 pixels per millimeter. This is also true for images with a magnification of 1:1. Thus the number of pixels per millimeter is a direct measure of the magnification of the optical system.

Locating the first maxima in the spectrum one can calibrate the length scale due to a certain number of pixels. The mean value of this procedure turned out to be 244 pixels per millimeter. Small deviations of this value on the order of 2 pixels lead to a completely shifted spectrum. This procedure is therefore much more exact than counting pixels on the actual image. The magnification of the system is the ratio of the number of pixels per unit

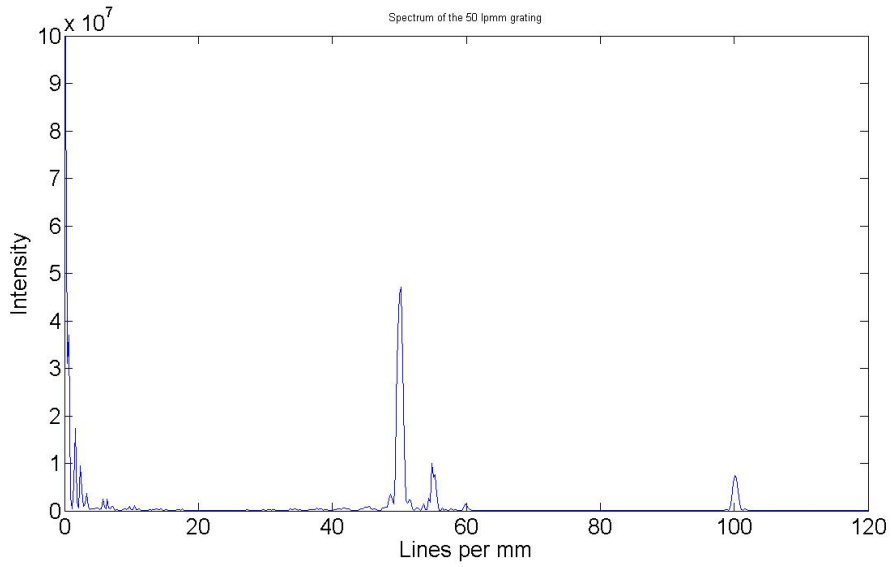

Figure 3.3: A Fourier transform along a line of a picture taken from the 50 lines per mm grating. The first order harmonic peak is used to calibrate the spectrum. The third order harmonic can be seen at 100lpmm. The peak at 55lpmm is due to the fact that a part of next grating with this spatial frequency can be seen on the original picture.

length of an image without magnification and and this from a magnified image. The ratio 155 : 244 leads to a magnification of 1:1.57 and a pixel size of 4.1μm×4.1μm of an imaged object.

3.2.3 Calculation of the modulation transfer function

Having a calibrated length scale it is possible to do further investigations of the spectrum obtained by the fast Fourier transform. The modulation transfer function (MTF) relates contrast, which is defined as the intensity difference between the maximum of the signal and the background, with the resolved spatial distance. therefore contrast is the height of the first harmonic in the spectrum. The intensity of the light source was high enough to get also a relevant signal of the third order harmonic at two times the spatial frequency. So it was possible to compare those two contributions and check for defocus or interferences with signals of neighboring line structures of the grating. The MTF was obtained by convolution of the first order maxima heights with four times the third order heights, the latter acting as a weight

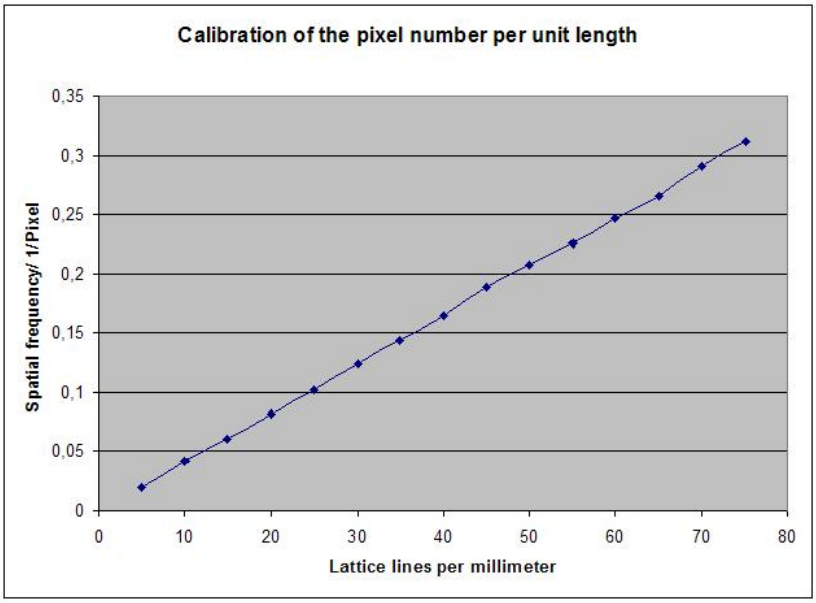

Figure 3.4: Calibration of the pixel number in comparison to the spatial frequency of the test grating. The linearity of this relation leads to a very exact method to determine the magnification of the optical system.

function representing deviations from the ideal image. The factor four is the ratio of the neighboring maxima in the ideal sinc-function.

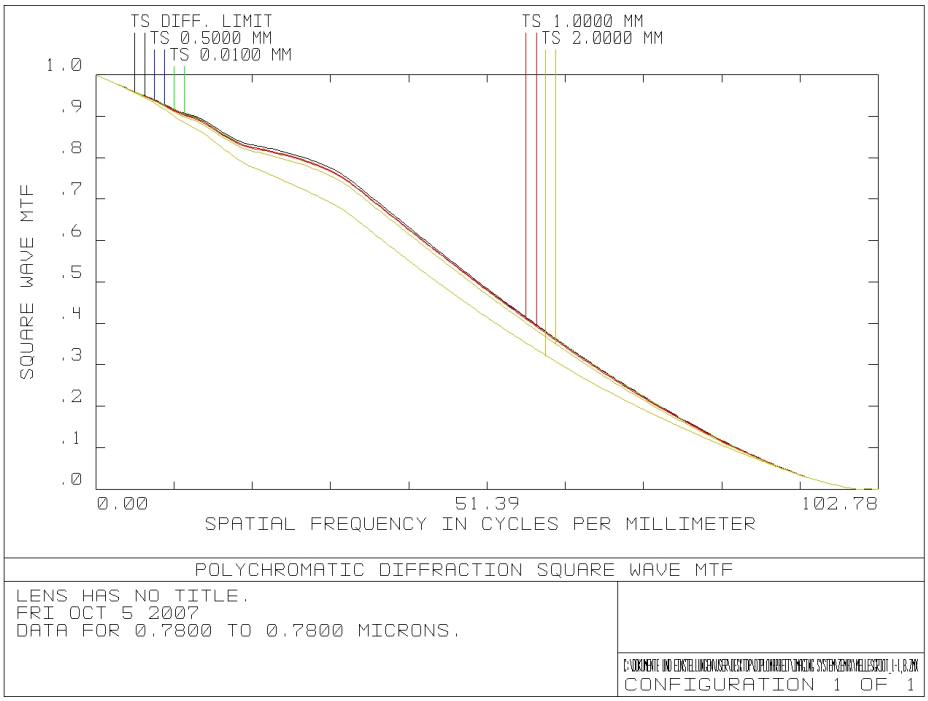

Figure 3.5: Simulated modulation transfer function by Zemax

3.2.4 The focal depth of the imaging system

The procedure of getting the MTF is applied to images taken of the test grating with varied distances to the imaging system to obtain the depth of focus. Again the relation of the first and third order maximum is calculated and is plotted as a function of the distance to the focus. The focal depth is defined as the distance were the spot size gets bigger by a factor of $\sqrt{2}$.
The evaluation of the images leads to a value of about 400μm for the focal depth.

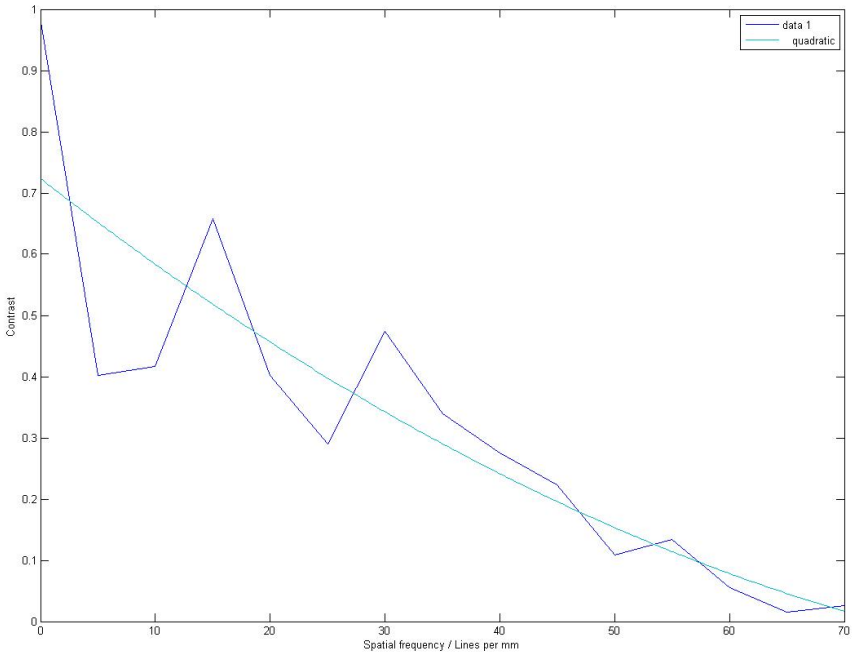

Figure 3.6: The measured modulation transfer function, obtained by the Fourier analysis of the test pictures. For each spatial frequency three pictures are taken with equal intensity and the first order harmonic is calculated which corresponds to the modulation of the intensity. The high deviation for low frequencies can be caused by higher order terms of lower frequent components matching with the modulation signal.

3.3 Imaging atoms

Dealing with cold atoms it is of interest to get the number of trapped atoms and the density of the atom cloud. This is important for evaporative cooling because during this process 99.9% of the atoms are thrown away. This can be done by evaluating pictures of the whole atom cloud. The atom cloud can be imaged by taking pictures of their fluorescence light after irradiating them with a laser beam or by taking pictures of the absorption of the laser light passing the cloud. This so-called absorption imaging is done by shining in laser light under a small angle of about four degree relative to the chip surface. Thus the imaging system installed under the same angle on the opposite side of the vacuum chamber takes pictures of the absorbed light by the atoms of the reflected beam and reflected light of the absorbed beam.

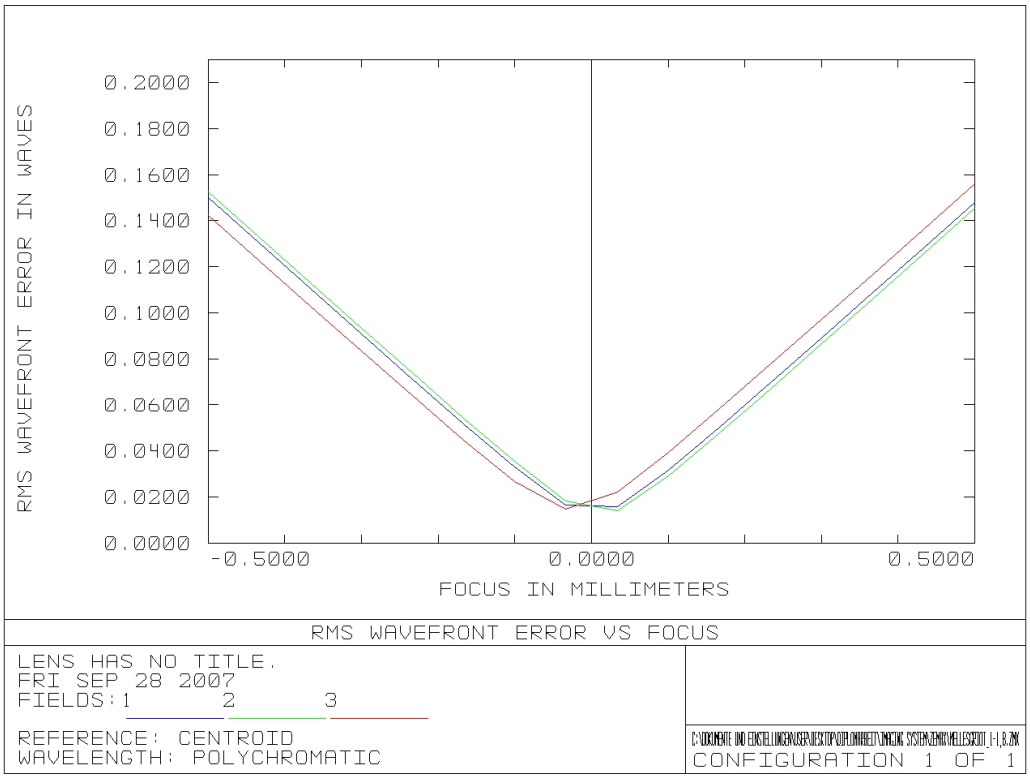

Figure 3.7: Simulated spot size in relation to the distance to the focus

This leads to the characteristic absorption imaging pictures, where the cloud and its mirror image is seen. This is done to have a measure for the distance of the atoms to the chip surface. Later on, when the loading behavior is understood the imaging system can be tilted to observe the cloud directly.

The imaged absorption profile can be used to estimate the number of atoms.

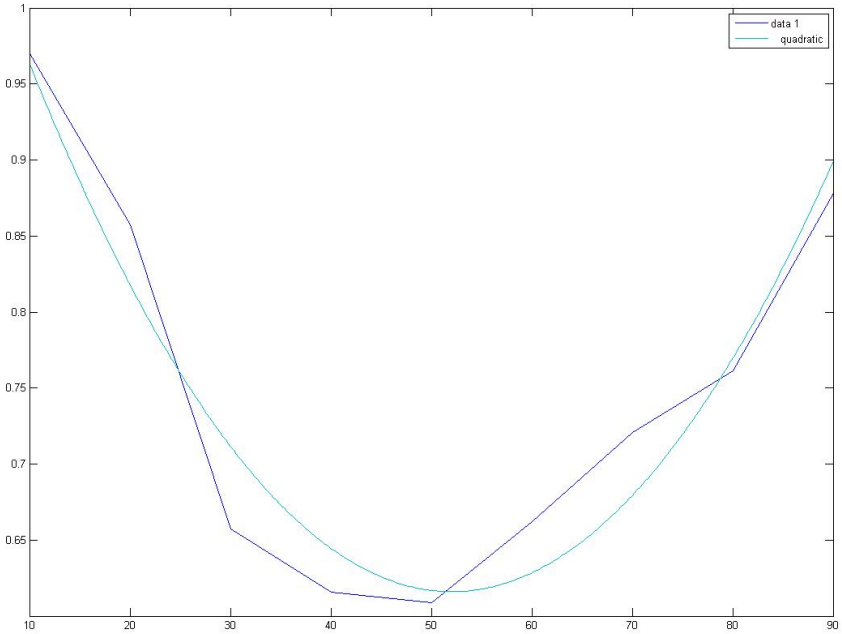

Figure 3.8: Focal depth of the system measured by the intensity drop of the first order harmonic of the test pictures in comparison to the third order harmonic. This is done for a series of pictures of the test grating driven through the focus.

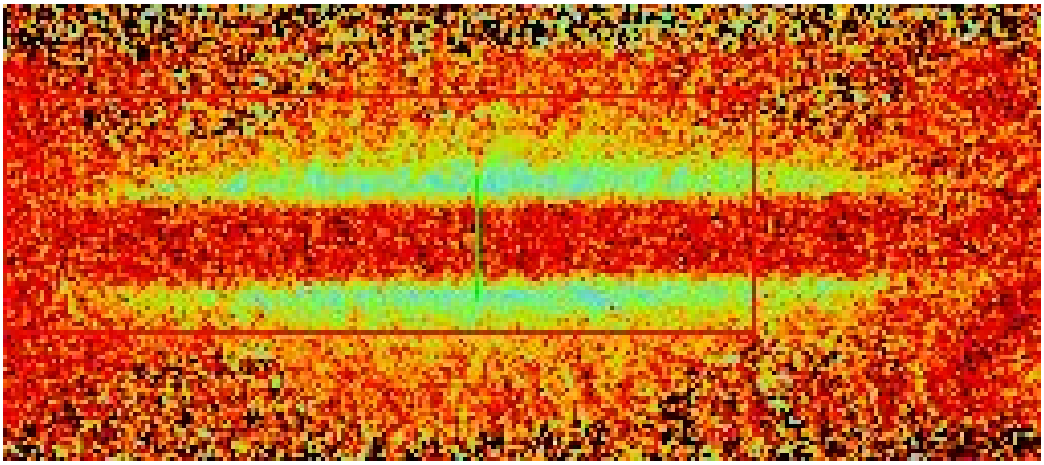

Figure 3.9: Absorption image of a cloud of trapped rubidium atoms on the micro-optics' chip Z after 210ms since loading into the trap. For absorption imaging the characteristic mirror image of the atom cloud can be seen.

Chapter 4

Optical lithography for micro-fabrication

In order to create geometrically well-defined electronic or optical devices nowadays the method of contact lithography is used. This process is the basis of the rapid progress in miniaturization of todays' technology. The big advantage of lithography is a high resolution due to the fact that in the near field regime Rayleigh's limiting criterion is no longer fulfilled. Resolution is only limited by Abbe's law where it has to be of the same order as the wavelength of the light in use. The atom chip contains structures of very large areas. In order to obtain these structures with good quality a so-called lift-off process is used. A silicon wafer is covered with a negative photo resist. Negative means that those parts exposed with UV-light remain while the unexposed parts are removed during development. The advantage of a negative resist is the undercut of the edges of the resist. By evaporating or sputtering the wire material onto the surface with the developed resist it is spread on top of the resist and it hits the gaps, where the resist is removed. If the aspect ratio of these gaps is high enough the undercut will guarantee that the final wires on the chip have well defined edges. After deposition of the wire material on the surface, the photo resist with the material on top of it is removed with the aid of a solvent.

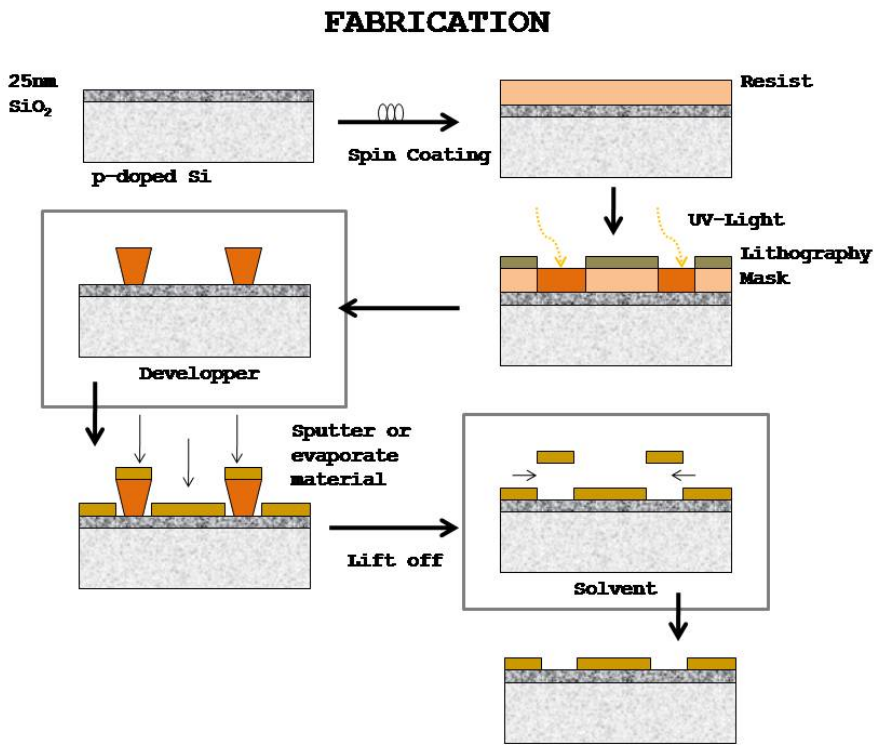

Figure 4.1: Typical fabrication steps

Three projects are carried out using micro-fabrication during this thesis, namely the fabrication of single layer atom chips, the construction of holding structures for micro-optics and a first test fabrication of superconducting resonator structures. Most of the fabrication steps are done in the clean room of the ZMNS(Zentrum für Mikro- und Nanostrukturen) Vienna.

Chapter 5

Fabrication of an atom chip

The atom chip is a very suitable tool for manipulating atoms because various shapes of electromagnetic potentials can be manufactured.

5.1 Design of an atom chip

There are several configurations of gold wires on the chip for different purposes. Many ideas have been brought up and realized up to now[22, 19, 13]. But there are three main structures for manipulating atoms, namely the side guide, the Z-trap and the U-trap. These three structures are combined with an external bias field. The most simple configuration is the side guide, which is a straight wire producing a confining field in the two dimensions perpendicular to the wire. Thus it is not a full trap for atoms because it leaves a degree of freedom along the wire, which has to be compensated by an external inhomogeneous field closing the trap. The side guide is often used to move the atoms on the chip. The U-trap is built of a double-bent wire and an external homogeneous bias field. This configuration produces a quadrupole trap with its minimum at the center of the U-shape. Because it contains a field zero the U-wire can not be used in this simple way to trap atoms due to Majorana spin flips. It is often used in a H-shaped structure, where two U's are opposing each other, which can be used to compress an atom-cloud in order to increase the phase space density. It is also used for a forced transport of atoms in a conveyor belt structure, where several opposing U-wires are displaced by half the width of the U. The most important way of trapping is the Z-wire. Because the two wires leaving the trapping region are bent into the opposite directions there is no vanishing field in the center and in combination with an external bias field this configuration leads to a Ioffe-Pritchard type trap.

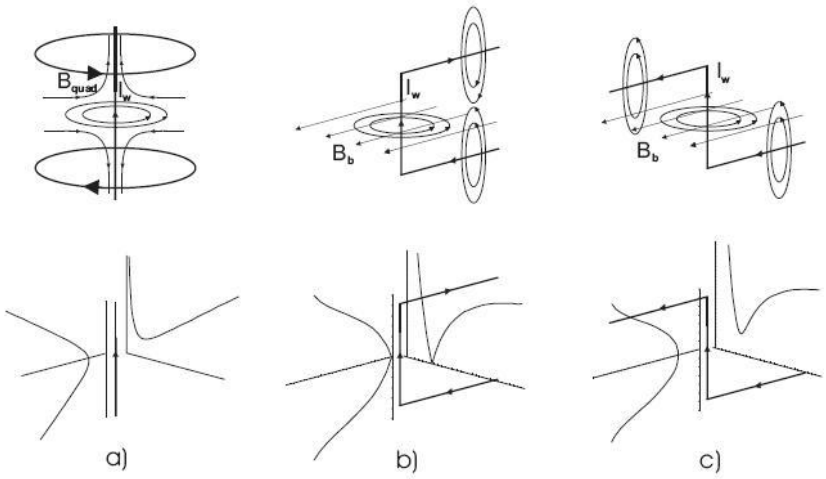

Figure 5.1: The three most simple trap geometries: a)The side guide, b)the U-trap and c)the Z-trap.

For the design of an atom chip several things have to be considered. The program in use in the moment is L-edit. With this polygons can be defined as metal structures on the surface of the substrate. For the production of the lithography-mask one has to think of the resist in use. Usual chips are built with a lift-off process, which means that the resist has to stay where no metal structures should appear, and usually a negative resist is used, which remains where it is exposed. Thus for a usual chip the chrome structures on the lithography-mask have to be placed where the metal wires will sit on the final chip. Because the atom chip should be a good mirror to reflect for the MOT-beams gold areas should be designed as large as possible. Another point to consider is that there is a limited number of contact pads on the chip, where the wires are bonded to the external current sources on the chip mounting. Thus it is the most common way to start the design by considering the number of wires needed and if there is a way to connect them all to the pads. Then the wires are broadened where it does not disturb the field configuration in order to increase the gold area. Finally one has to design cutting lines around the chip to define an edge for the cutting process. If there are other structures that require another lithography step it is useful to design special structures on both masks for alignment.

5.2 Fabrication of a single layer atom chip

This process was developed by Martin Trinker at the ZMNS Vienna as an adaption of Sönke Groths process[15, 14, 12]. The fabrication process of the single layer atom chip is as following.
First a p-doped silicon wafer is ordered with a 25nm layer of silicon oxide. The dotation increases the heat conductivity of the substrate and therefore the heat produced by the wires is transported away faster. On the other hand the silicon oxide covering enhances its electric isolation properties. The wafer is broken into pieces with desired size by hand. At first a small cut is scribed at the edge of the wafer with a diamond scriber. Then it is held and broken like a catholic priest holds and breaks bread directly before the communion. It has to be made sure that there is at least 5mm overlap at the edges of the chip for demolitionless handling of the substrate.
After blowing away possibly occurring dust with the nitrogen shower the substrate has to be cleaned. At first it is put in distilled water into the ultrasonic bath, then it is rinsed with acetone and isopropanol and finally it is dried on the hot plate.
The negative resist in use for the atom chip is AZ nLof2035 for its very suitable properties. It has very stable and reproducible processing parameters and its aspect ratio of up to four combined with an undercut leads to very sharp structured wires. The resist is spread on the substrate with the help of a syringe and spin coated for 35s with a spin speed of 4000rpm. This leads to an approximately 3μm thick film with which 2μm wide structures can easily be resolved. It is possible that the resist is thicker at the edges of the substrate due to the centrifugal force. This so-called edge bead could prevent full contact of the resist with the lithography mask. It can be removed by going around the edges with a q-tip soaked in acetone.

For the exposure the chrome mask with the desired structures is installed in the mask aligner. The chip is put on the sample holder and aligned with the mask. Then it is exposed with a standard ultra violet light source with a wave length of 365nm for 7 seconds which corresponds to an exposure dose of $84 mJ/cm^2$. At this point it is possible once more to get rid of dust by nitrogen showering the sample.
The chip has to be placed on the hot plate at 110 °C for 1 minute for post exposure bake to finish the cross-linking process of the exposed parts. The resist is very sensible to this parameters and they had to be found out empirically.
After cooling the sample to room temperature it is developed by rinsing it in AZ 326MIF for 70s. The developing process should be visible at about

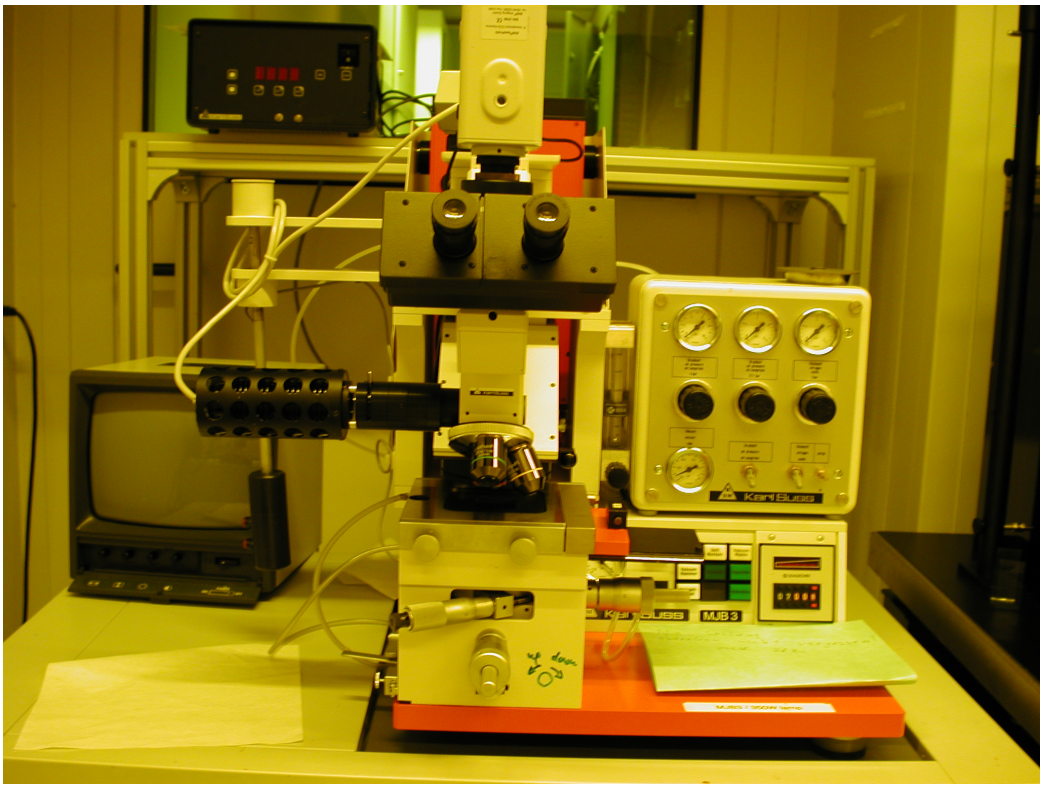

Figure 5.2: Mask aligner Suss MJB 300: A 300 Watt light source with the two typical wave lengths 365nm and 405nm for optical lithography. The mask and the sample are put into contact and the UV lamp is driven over them during exposure. The power of this light source is $12mW/cm^2$.

30s. After that the chip is rinsed in distilled water and blown dry with the nitrogen shower. It was found out that possible remainders of the unexposed resist can be burnt away by the plasma cleaner. The chip is put into it after development for 3min at 300 Watt.

The gold layer is thermally evaporated onto the chip surface. It is installed on a sample holder above an evaporation crucible in a vacuum chamber. Two crucibles are loaded, one with titanium and one with gold. The chamber is evacuated down to $\approx 10^{-6}$mbar, then current is pushed through the titanium crucible until its content is melting. The evaporation process is controlled by the current through the crucible. A titanium layer of about 25nm is used to increase the adhesion of the gold layer because the adhesion of gold on silicon is very bad. Evaporating titanium has the further advantage that the vacuum is increased due to the gettering properties of this element. After this the

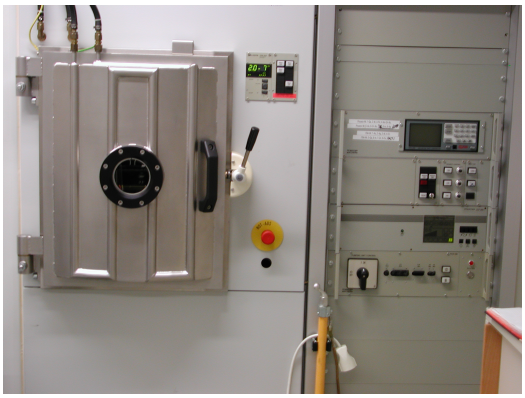

Figure 5.3: Balzers evaporation device: The evaporation process is started at a pressure of 10^{-6} mbar. The current for the evaporation is controlled by a potentiometer at the control panel. The indicator for the deposition rate also situated there has to be calibrated by a factor of 7, because the sample holder is mounted nearer to the evaporation source than that for usual samples.

Figure 5.4: Modified sample holder in the evaporation device. The original one is the surface located in the upper area, the new one is that in the central area.

evaporation procedure is repeated with gold until the desired layer thickness is achieved. For the fabrication of atom chips a special sample holder is designed and installed which decreases the distance of between the sample and the crucibles. This is done to get faster evaporation rates and to reduce the needed amount of gold. For this reason the thickness indicator at the evaporation device has to be recalibrated by a factor of ≈7. The evaporated layer thickness is measured by a piezo-crystal whose eigenfrequency changes due to the change of its mass. For titanium one pallet is more than enough and the boats where it is molten in the crucible can be reused in order to save titanium. For the gold layer 1.5g of gold is needed per 1μm layer thickness. After evaporation the resist and the gold layer on top of it has to be removed with the help of a solvent. This process, where the solvent crawls under the gold structure, is called lift-off. The chip is placed slightly tilted with the upside down into a glass of NMP, which is a very effective organic solvent. The lift-off process can be accelerated by putting the glass onto the hot plate at 140°C or into the ultrasonic bath. By combining these techniques a successful lift-off of all unwanted structures was observed after 1-2 hours. But to be assured of having a proper lift-off the samples were usually left in NMP overnight.
In order to protect the chip during cutting the edges it is covered with AZ5214 resist by spreading it onto the surface and spinning it with 500rpm for 1 min. The chip is cut with a diamond saw situated at the Institut für Sensor- und Aktuatorsysteme. Then the protective resist is removed by putting the chip on the spin coater and rinsing it with acetone and isopropanol during spinning.

5.3 The chip trap

There are several reasons to do physics of ultra cold atoms near a surface with electromagnetic devices on it. Some of these reasons have been already mentioned in this thesis. At first it is of interest to test all kinds of potentials for an atomic ensemble. Another advantage of micro-fabricated devices are geometrically well manufactured potentials providing high field gradients. Thus there is the possibility to confine the atoms in order to obtain a low dimensional quantum system. A further development is to invert experimental situation by using ultra cold atoms as a high definition probing device for the electromagnetic field produced by the surface structures. Finally it is the striking concept of the so-called mirror-MOT, being a rather easy method of cooling and trapping atoms near a surface. After cooling down the atoms and trapping them with a Ioffe-Pritchard type trap produced by external

coils on the outside of the vacuum chamber, they have to be transported to the magnetic trap on the chip. This is either done by loading the atoms directly into the trap on the chip or by using a step in between, where the atoms are loaded into a trap produced by a solid copper structure. The second method has the advantage that the atom cloud can be further cooled and compressed before it is loaded onto the chip increasing the phase space density there.

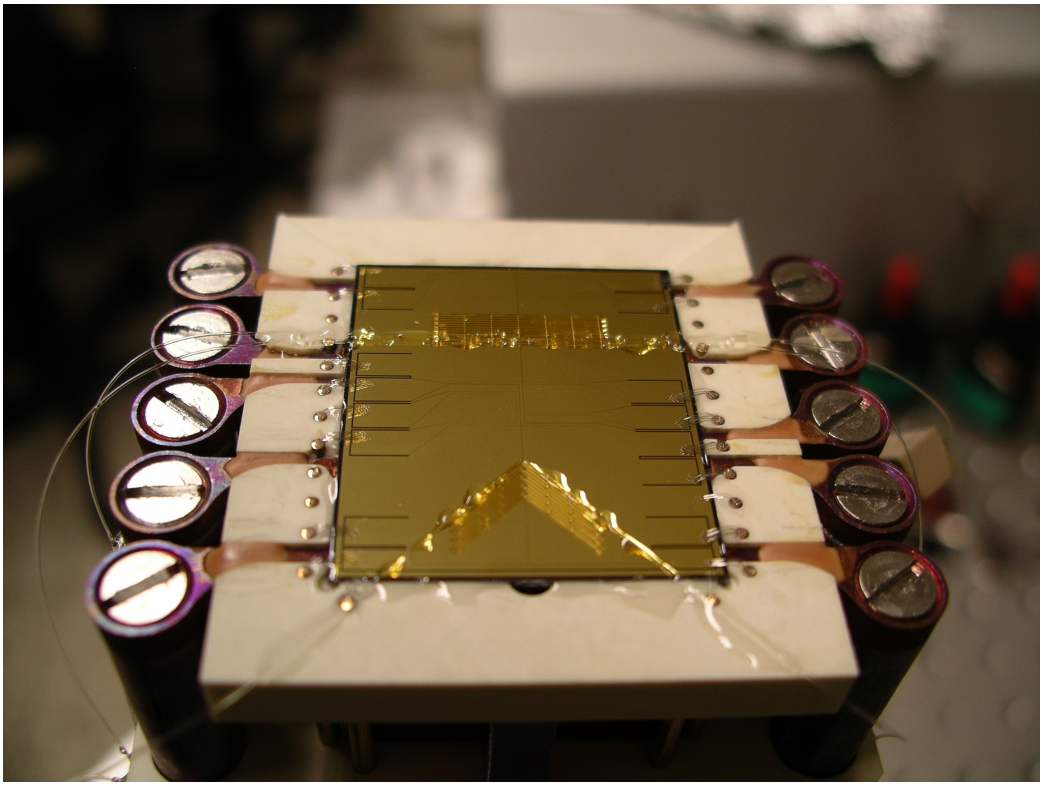

Figure 5.5: The old micro-optics chip with integrated fluorescence detectors

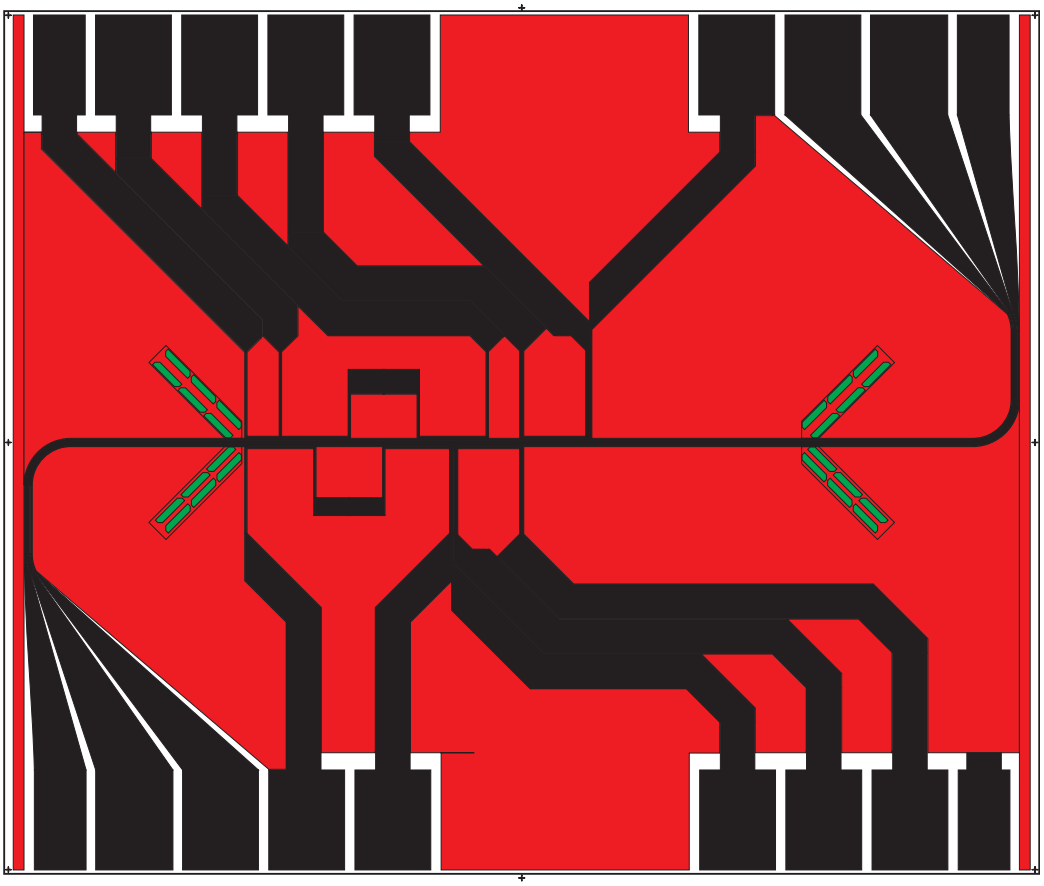

Figure 5.6: Design of the new micro-optics chip with integrated fluorescence detectors

Chapter 6

SU-8 holding structures for integrated micro-optics

6.1 SU-8 - A photoresist for high aspect ratio micro structures

SU-8 is used on a wide range of different fields of today's technology, especially in the telecommunication sector. Its chemical properties [23], containing an oligomer built of eight epoxy groups and a photoacid generator, leads to thermally and mechanically stable structures after exposure with ultraviolet or higher-frequent light and heating. The irradiated acid acts as catalyst for the cross-linking process of the epoxy groups. Thus the exposed parts of the resist stay after development while the other parts are removed. There are different types of SU-8 available which can be distinguished by their viscosities and the solvent in use. Therefore these different mixtures are made for different applications with differing thickness of the final structures and differing baking times. These recipes are labeled by a number after the term "SU-8", which represents the medium it is solved in and the order of the possible thickness in micrometers[7].

6.2 Influencing the undercut of the structures

Different parameters are influencing the shape of the final SU-8 structures and in general these parameters are depending on each other nonlinearly. In order to obtain these dependences a test structure was designed, which looks similar to those of which the planned final structures on the chip will be built of. This is a simple rectangle with a length of 2000μm and a width

of 200μm. A whole array of these rectangles were written on a test mask, where the distances between them were varied around the diameters of the two different fibers. One array was designed for the fiber with a diameter of 230μm varying the gaps in between the structures by 2.5μm starting from a width of 190μm and ending up at 230μm, the other array varies by the same step size from 90μm to 125μm, the diameter of the smaller fiber.

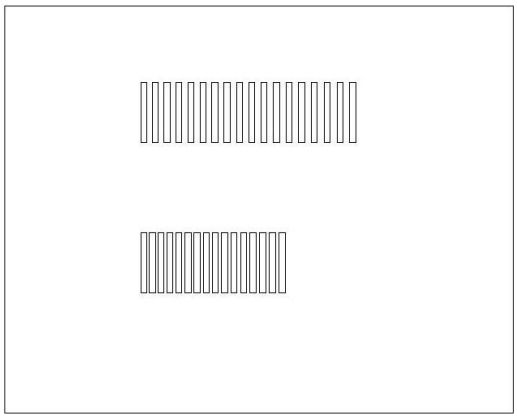

Figure 6.1: Lithography mask for SU-8 test structures: The upper structures are made to test the 230μm fiber and the lower ones are for the 125μm fiber.

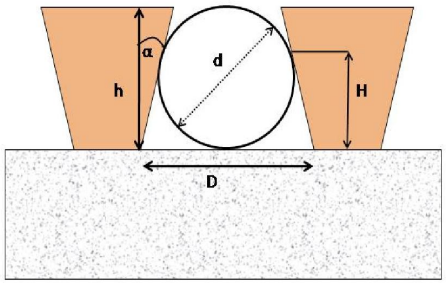

Figure 6.2: Geometrical properties of the fiber in between the SU-8 strucures.

Both fibers should fit into the structures as tight as possible. Thus the undercut angle α is related to the bottom distances D of the structure by the trigonometric expression

$$D = d \cot \frac{\alpha}{2}, \tag{6.1}$$

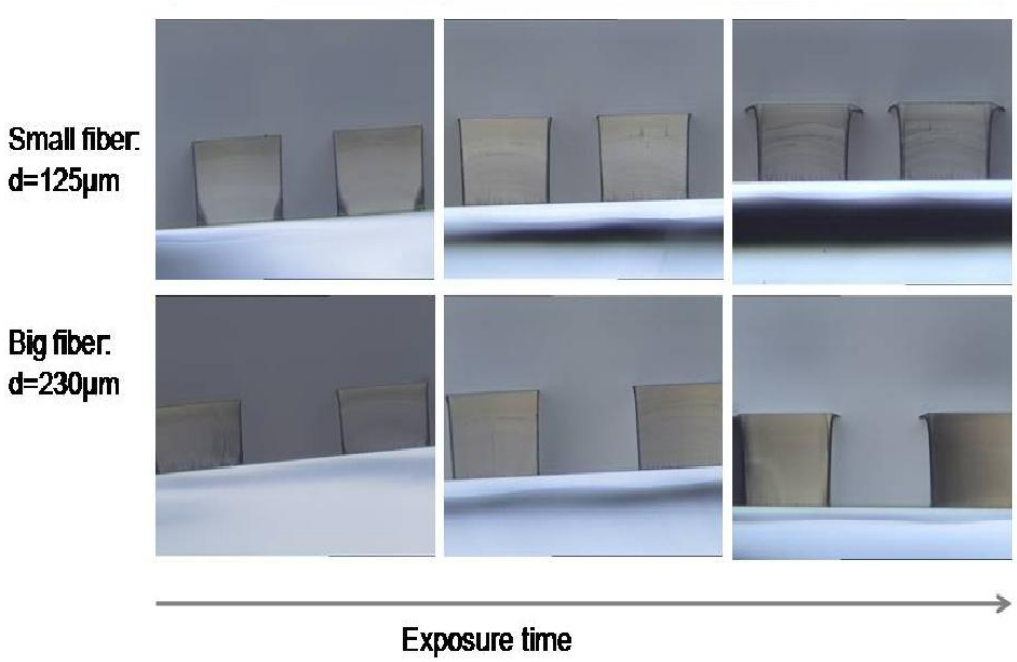

Figure 6.3: The undercut in relation to the exposure dose. There is an undercut for underexposure, which is getting smaller with increasing dose until it vanishes at $\approx 400 mJ/cm^2$ seen in the central picture. Going to even higher doses leads again to some angle in the side walls and the characteristic T-topping for overexposed structures.

with the diameter d of the fiber used. Another important value is the height where the fiber touches the structures, since this defines the minimum thickness of the resist. This height H can also be related to the angle

$$H = d \cos \alpha \tag{6.2}$$

This relation leads to a minimal height of about 120μm for the big fiber. In order to guarantee mechanical stability of the fibers in the holding structures at least 20% of height is added to this value. Thus a thickness of the resist was chosen to be at least 160μm.

At first the spin coating process had to be calibrated. This was done by going through several values of the rotation speed, where it was looked to obtain a height of 160μm. The samples were broken perpendicular to the rectangular structures to look at the cross section under the microscope.

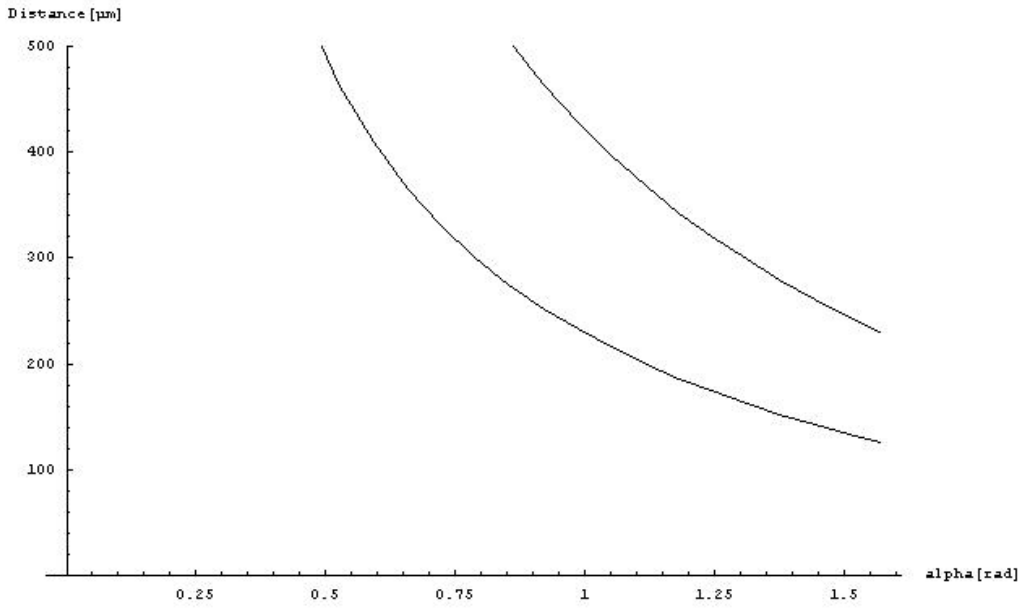

Figure 6.4: The bottom distance of the SU-8 structures for different undercut angles. The 230μm-fiber is described by the upper curve and the 125μm-fiber by the lower one.

There the height of the structures could be measured with an integrated length scale in the ocular. The thickness is approximately proportional to the inverse square of the rotation speed.

For there were problems with the sample sticking to the mask during the exposure process the prebake time was increased up to three hours. This seems to solve the problem without getting any negative side effects such as thermal destruction of the resist. Thus the exposure dose was the only parameter left to control the undercut of the structures. There exist models[8] to describe the different shapes of the structure's side walls due to the exposure dose and the air gap between the sample and the mask. But the fact that there is a nonlinear dependence on several parameters and that the sample is built on top of a gold mirror changes the exposure behavior in an unpredictable way. The most counterintuitive result during the exposure of the resist concerned the lateral distance between the final SU-8 structures.

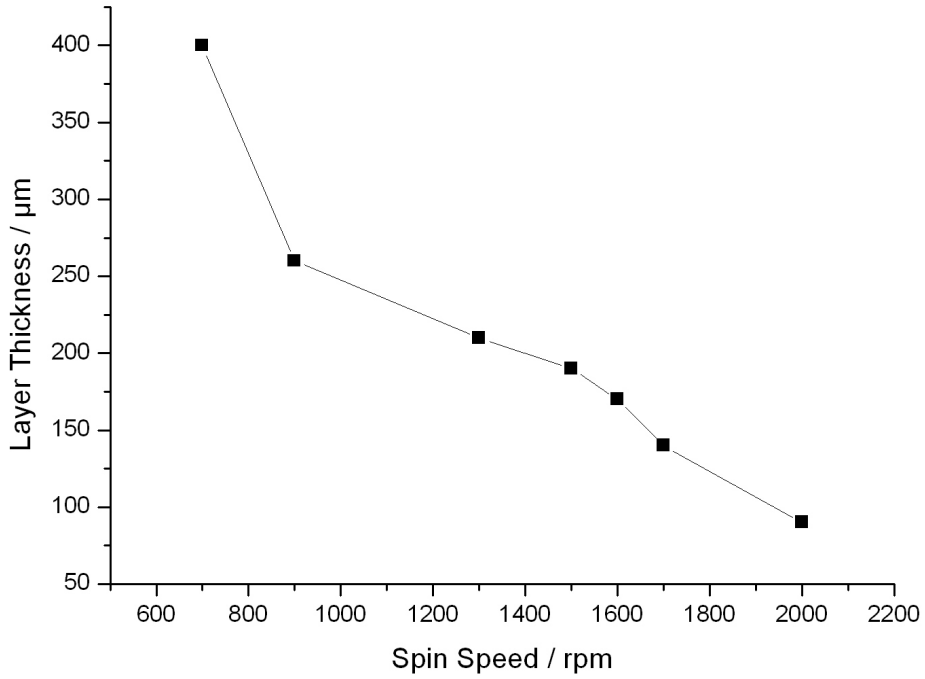

Figure 6.5: The calibration of the spin coating process for high SU-8 structures

The lithography-mask turned out to define the distances at the bottom of the structures right at the gold surface. The negative slope of the side walls, which is an effect of near field diffraction at edges of the mask, is called undercut. The walls are hanging over the empty regions of the substrate and these regions are defined by the chrome evaporated parts of the lithography mask.

6.3 Lithographic processing with SU-8 50

For our purposes a thickness of at least 160μm was required. Because of the fact that there was only SU-8 50 available, the parameters for the lithographic process had to be found.
The final process is described in detail in the following. In order to clean the substrate it is rinsed in distilled water and dehydrated on the hot plate for 1h at 200 °C immediately before use. This step is necessary to increase the adhesion of the resist on the gold coated substrate. After cooling to room temperature SU-8 50 resist is spread on the surface of the substrate. Because of the resist's high viscosity it is preferable to pour it on the chip directly from the bottle instead of using a pipette. Small air bubbles may occur if the resist is too cold. These bubbles usually disappear during the prebake process. A suitable technique to get rid of these is to pour much more resist onto the surface as necessary.

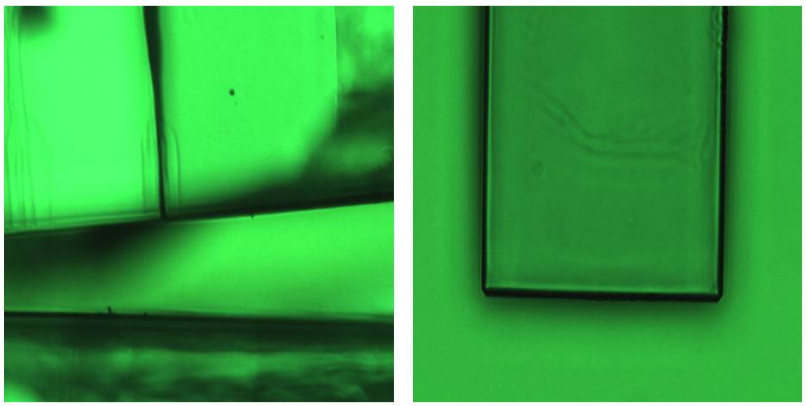

Figure 6.6: Broken SU-8 structures due to underexposure with only $160mJ/cm^2$(left). Top view of an intact structure with a magnification of 1:10(right).

The desired thickness of the coating is achieved by spinning the substrate at 500rpm[1] for 20s, followed by 1500rpm for 20s. This produces an approximately 160μm thick film.

[1]abbr. **r**evolutions **p**er **m**inute

The resist has to be prebaked in order to evaporate the solvent out of the sample. A balance has to be found between baking to short on the one hand which leaves the resist in a consistence where it is likely to stick at the lithography mask and baking to long which can cause thermally induced cracks in the final structure. Thus it is put on the hot plate for 65 °C for 10min, then the temperature is ramped up to 95 °C during a time of approximately 6min and finally held constant for 3h.
After cooling to room temperature it is exposed with a standard 365nm UV light source with a dose of 400mJ/cm^2 or less to get the desired undercut of the structures.
The sample is postbaked for further cross-linking of the exposed oligomers on the hot plate first at 65 °C for 1min, then the temperature is ramped to 95 °C during a time of 2min and held for 9min. These ramps during baking are necessary to avoid sudden temperature steps, which can partly destroy the structures. It is also recommended to avoid sudden cooling to room temperature by putting the sample into contact with a good heat conducter.
After cooling to room temperature the unexposed parts are removed by rinsing in SU-8 developer(PGMEA) for 12min, then in isopropanol for 1min and finally in distilled water. If the removal process is not finished the unexposed resist is seen flowing away in isopropanol. If this happens it has to be put back into the developer and it may be useful to take a fresh developer due to saturation of the old one.

6.4 A single atom fluorescence detector

The current setup and evaluation of the single atom detector is explained in detail in refs [20, 21]. SU-8 holding structures are installed to align two optical fibers under an angle of 90∘. In the actual setup both fibers have a diameter of 125μm. The laser light coupled into a single mode fiber is focused onto a guiding wire with a tapered lens on its end. Ultra cold atoms produced in a Z-trap are loaded into the guide and transported into the focus of the detector and absorbs photons. The multimode fiber sitting on the other side of the guide collects the re-emitted photons. Decreasing the photon intensity and the average number of atoms in the guide one can observe single atoms being single photon emitters, due to the fact that the atoms need time for an absorption-emission cycle. The emitted photons are counted with an avalanche photo diode. The new chip and the new detectors will have in principle the same design. There will be multimode fibers with a diameter of 230μm to increase the photon collection rate. For this purpose a new process for the SU-8 structures had to be found in the course of this

thesis.

old.pdf

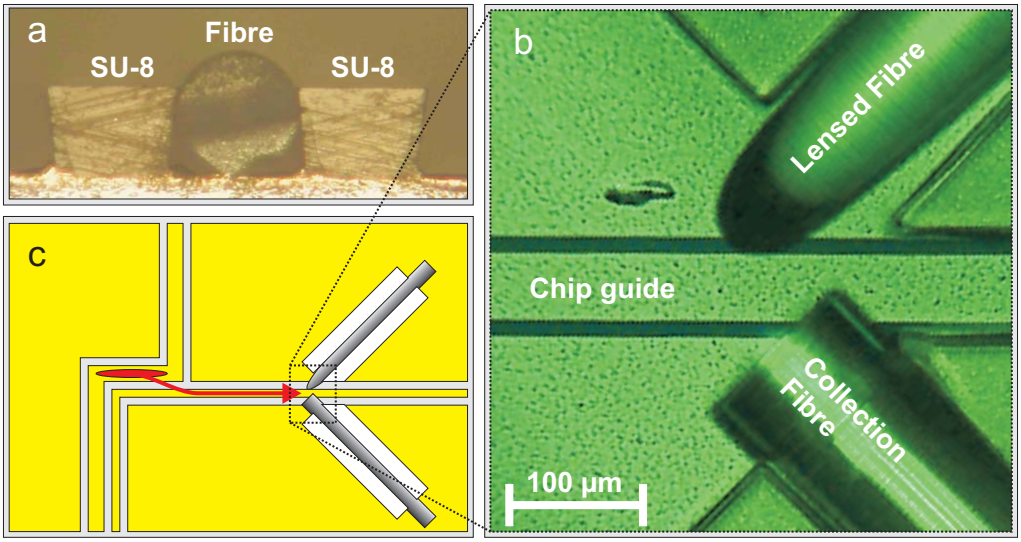

Figure 6.7: The current micro-optics chip: The atoms from the Z-trap are loaded into a guide transporting them to the fluorescence detector. The light shone in from the tapered lensed fiber is absorbed at the fiber's focus by atoms and the re-emitted light is collected by the multi-mode fiber.

Chapter 7

Superconducting niobium microwave devices

A very recent project is the implementation of an interconnect between superconducting solid state q-bits like Josephson-junctions and ultra cold atoms. This is done with the help of a coplanar wave guide for micro waves built of niobium, which is a superconductor [10, 11]. In order to obtain superconductance a cryostatic environment is needed. The interconnect is done by coupling both solid state qubit and atom to the modes of a transmission line resonator. For a first test of the fabrication process with niobium test resonator structures are built.

The fabrication steps are similar to those of an atom chip described in detail in chapter 5. After cleaning and spin coating with AZnLOF resist of about 3μm thickness, it is pre-baked, exposed and post-baked. Then, after it is developed, niobium has to be deposited on the chip. Due to the fact that niobium can not be evaporated it has to be sputtered onto the substrate. For this process the sputtering rate had to be determined. The sample is evacuated in the sputtering device to $\approx 10^{-5}$. After a radio-frequency fed plasma has ignited, argon ions are accelerated towards a niobium target, which causes a sputter process of niobium and finally its deposition on the chip.

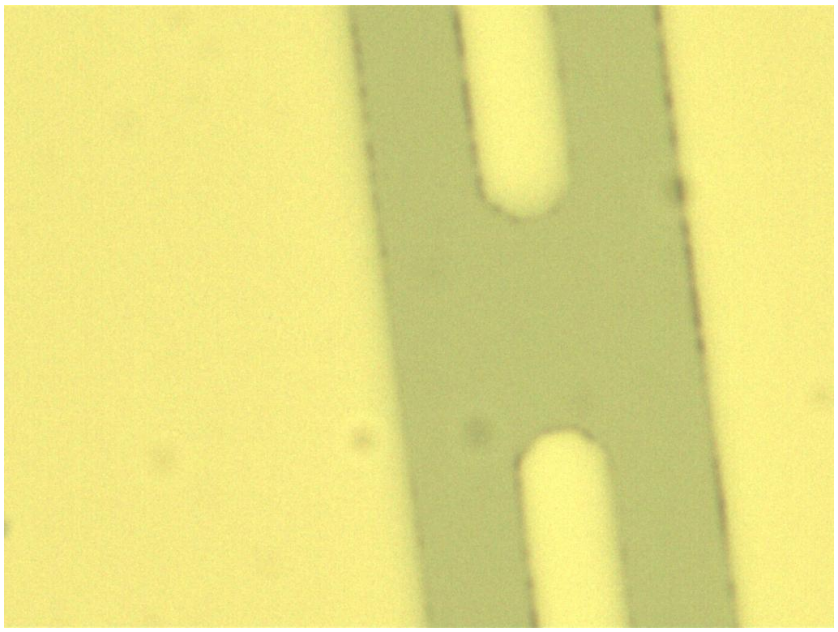

Figure 7.1: Detail of a niobium resonator structure at a magnification of 1:100. This is one of the mirrors in the coplanar wave guide with a width of 2μm. The height of this structure is estimated to 2μm.

The sputtering process done in steps of 60 seconds with a cooling step of the sample in between. This prevents the resist from being burnt away. The total sputter time was increased until the height of the structures reached the thickness of the resist which can easily be observed under the microscope because the lift-off process does not work any more. This leads to a first estimation of the sputter rate. Assuming a linear sputtering process, the rate is $\approx 0.7\mu$m per minute because the height of the resist is reached after 4 steps of 60s. For a proper determination of the sputter rate, the height of the structures have to be measured with a profilometer.
After the sputtering process the usual lift-off is done with NMP. The result of these first test steps is that optical lithography and the lift-off process can be used to fabricate niobium resonator structures. For smaller structures like q-bits beyond the optical regime, electron beam lithography has to be used and an etching process like reactive ion etching.

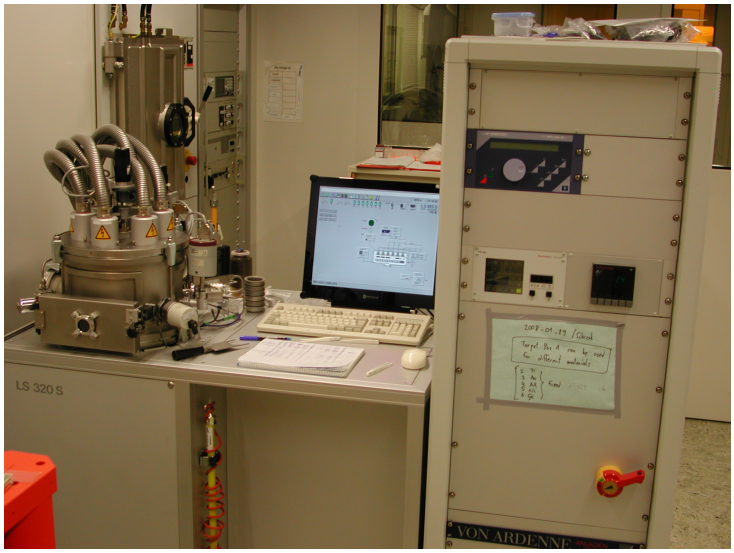

Figure 7.2: Sputter system: The samples are evacuated in the chamber to the left. The niobium target is built into one of the electrodes situated in the upper part of the chamber.

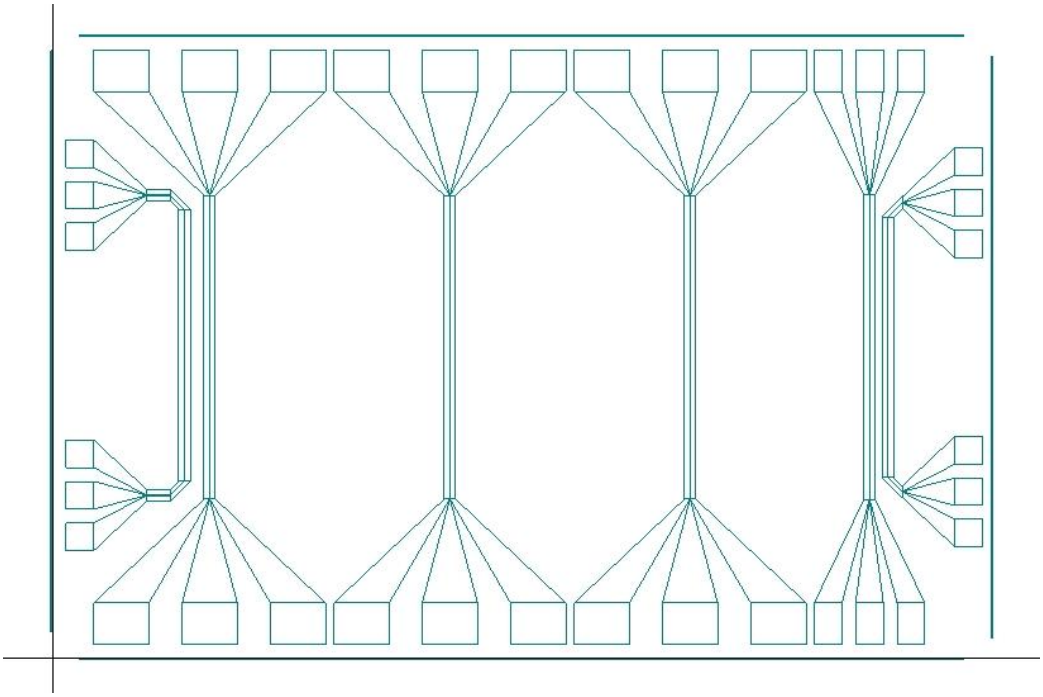

Figure 7.3: Test design for the microwave resonator containing coplanar wave guides with cavity mirrors on it.

Conclusion and outlook

Different processes of fabrication are discussed in this thesis. There are two ways to categorize them, namely by the way the device is fabricated, which leads to the development or continuation of fabrication techniques, or by the purpose for which it is fabricated, which leads to a characterization of a certain device for this purpose.
Using the latter description for this thesis one can distinguish optical devices for the detection of ultra cold atoms and electromagnetic devices for trapping and manipulating atoms. An optic system is built and characterized for the purpose of imaging ultra cold atoms. The system is a rather simple one containing two lens doublets. Its characterization was done with the help of Fourier optics by evaluating CCD pictures of a resolution target with well defined spatial properties. As a result the resolution of the system is described for all spatial distances down to the resolution limit of the lens system found for this system at 9-10μm both experimentally and by simulation. The focal depth of the system is evaluated and found to be 400μm, which is a bit more than it comes out of the simulation.
As a second optical device a new fluorescence detector will be built with the help of micro-optics on the chip. In this thesis the structures to hold and align the optical fibers used for the detector are designed and the fabrication is tested. The old, slightly different, design turned out to work quite efficient in the detection of atomic fluorescence photons.
The electromagnetic devices are the standard single atom chip containing micro-fabricated gold wires and the superconducting transmission line resonator. Whereas the atom chip is a well understood and characterized device for trapping, cooling and manipulating atoms, the transmission line resonator is not characterized yet for the purpose it is produced, namely coupling atoms to solid state quantum devices.
A second goal of this thesis was to learn about today's techniques of microfabrication with the help of optical lithography and to use them for the needs of an atom optics group. Thus it concerns the first category mentioned above, namely fabrication. The design of a lens system is done with a ray tracing

simulation program and it is built with standard off-the-shelf lenses and mountings usually used in a quantum optics group. The other devices are fabricated in the cleanroom of the Zentrum für Mikro- und Nanostrukturen Vienna. This work included optical lithography and physical vapor deposition, namely sputtering and evaporation, handling with samples in a clean environment. Meanwhile he fabrication of the atom chip is well understood and a very stable and reproducible process. On the other hand the process of getting niobium structures onto the chip this way was not tested yet by any group in Vienna. Thus it was a task of this thesis to do a first test fabrication of these structures. As a first result the sputter rate for Niobium was tested and the lift-off process for resonator structures down to a size of 2μm being the limit of optical lithography turned out to work and to be controllable.

Chip Recipes

A baking instruction for SU-8 structures of 160μm on a gold coated wafer. A modified recipe of Liu et al[6]

.

1. Preparation of the substrate
    - In order to clean the substrate rinse it in distilled water.
    - Dehydrate it on the hot plate for 1h at 200 °C immediately before use.
2. Coating
    - After cooling to room temperature spread SU-8 50 resist on the surface of the substrate by gently tilting the bottle.
    - Spin the substrate at 500 rpm for 20 s, followed by 1500 rpm for 20 s. This should produce an approximately 160μm thick film.
3. Prebake
    - Prebake on the hot plate for 65 °C for 10 min, then ramp up to 95 °C during a time of approximately 6 min and hold it constant at this temperature for 2h.
4. Exposure
    - After cooling to room temperature expose it with a standard 365 nm UV light source with a dose of 400mJ/cm^2 or less to get the desired undercut of the structures.
5. Postbake
    - Postbake on the hot plate first at 65 °C for 1 min, then ramp to 95 °C during a time of 2 min and hold this temperature for 9 min.

6. Development

    - After cooling to room temperature remove the unexposed parts by rinsing in SU-8 developer for 12 min, then in isopropanol for 1 min and finally in distilled water.

Single layer Atom Chip recipe developed by M. Trinker

1. Preparation of the substrate

    - Break the SiO_2-coated Silicon wafer into a chip of desired size with approximately 5 mm tolerance at the edges.
    - Put the substrate in distilled water in the ultra-sonic bath, then rinse it with acetone and isopropanol and dry it on the hot plate.

2. Coating

    - Spread the AZ nLOF2035 photo resist on the surface of the chip.
    - Spin it with 4000 rpm for 35 s to obtain an approximately 3 μm thick film.

3. Exposure

    - Remove possibly occurring edge bead by going along the edge with a q-tip soaked in acetone.
    - Expose the coated substrate with the 365 nm UV light source situated at the ZMNS[1] Wien for 7 s, which is an exposure dose of 84 mJ/cm^2.

4. Soft bake

    - Put it on the hot plate at 110 °C for 1 min to finish the cross-linking process in the resist. Illuminate regions where the gold film should be removed after the lift-off.

5. Development

    - After cooling to room temperature remove the unexposed parts of the resist by rinsing the chip in AZ 326MIF developer for 80 s.
    - Rinse it in distilled water and dry it with the nitrogen shower.

6. Evaporation

[1] Zentrum für Mikro- und Nanostrukturen

- Put the chip into the plasma asher for 3 min at 300 Watt to burn the remainders of the unexposed resist.
- Evaporate titanium onto the chip surface to increase the adhesion of the gold structures until the thickness display of the Balzers evaporation device reaches 30 Å, which leads to a real thickness of ≈25nm due to the fact that the detection is wrong by a factor of ≈7 because our probe sits further away than usual ones.
- Evaporate 1.5 g gold per micrometer onto the surface. Do not forgot a factor of seven as explained before.

7. Lift-off

   - Put the chip into NMP[2] overnight to wash out the resist under the gold layer.
   - Heating and/or ultra-sonic bath may help to get rid of huge gold areas.

8. Protective coating

   - Prevent the structures from further damage due to the cutting process by coating the chip with AZ 5212 resist.
   - Spin the the chip with 500 rpm for 1 min.

9. Cutting

   - Cut the edges with a diamond saw.
   - Remove the protective coating by rinsing the chip during spinning with acetone and isopropanol. It is possible to remove some remainders of the lift-off process using a q-tip.

[2]N-Methyl-2-pyrrolidone

Bibliography

[1] Reider, G.: *Fourieroptik*, Skriptum zur Vorlesung, (2000).

[2] Hecht, E.: *Optik*, Addison-Wesley (Deutschland) GmbH, (1989).

[3] Foot, C.J.: *Atomic Physics*, Oxford University Press, (2005).

[4] Fox, M.: *Quantum Optics: An introduction*, Oxford University Press, (2006).

[5] Metcalf, J.M. ; van der Straten, P.: *Laser Cooling and Trapping*, Springer-Verlag New York Inc., (1999).

[6] Liu, X. et al.: *Fabrication of alignment structures for a fiber resonator by use of deep-ultraviolet lithography*, Appl. Optics **44**, (2005), 6857 - 6860.

[7] Microchem: *NANO^{TM} SU-8: Negative Photoresist formulations 50-100*, www.microchem.com.

[8] W.-J. Kang et al.: *Novel exposure methods based on reflection and refraction effects in the field of SU-8 lithography*,J. Micromech. Microeng. **16**, (2006), 821-831.

[9] Einstein, A.: *Zur Quantentheorie der Strahlung*, Physik. Zeitschr. **18**, (1917), 121.

[10] Schoelkopf, R.J. ; Girvin, S.M.: *Wiring up quantum systems*, Nature **451**, (2008), 664-669 .

[11] A. Palacios-Laloy, F. Nguyen, F. Mallet , P. Bertet, D. Vion and D. Esteve : *Tunable resonator for quantum circuits*, arXiv:**0712.0221**, (December 2007).

[12] M. Trinker, S. Groth, S. Haslinger, S. Manz, T. Betz, I. Bar-Joseph, T. Schumm, J. Schmiedmayer: *Multi-layer atom chips for versatile atom micro manipulation*, arXiv:**0801.3351**, (January 2008).

[13] S. Hofferberth, I. Lesanovsky, B. Fischer, J. Verdu, J. Schmiedmayer: *Radio-frequency dressed state potentials for neutral atoms*, Nature Phys. vol.2 **10**, (2006), 710-716.

[14] S. Groth, P. Krüger, S. Wildermuth, R. Folman and T. Fernholz, D. Mahalu, I. Bar-Joseph, J. Schmiedmayer: *Atom Chips: Fabrication and Thermal Properties*, Appl. Phys. Lett. **85**, (2004), 2980.

[15] S. Groth: *Development, fabrication, and characterisation of atom chips*, University of Heidelberg,(2006).

[16] S. Wildermuth; S. Hofferberth; I. Lesanovsky; E. Haller; L.M. Andersson; S. Groth; I. Bar-Joseph; P. Krüger; J. Schmiedmayer: *Microscopic magnetic-field imaging*, Nature **435**, (2005), 440.

[17] C. Barks : *Lustiges Taschenbuch*, ehapa-Verlag, **207**, (1992), 139-146.

[18] S. Aigner, L. Della Pietra, Y. Ja, O. Entin-Wohlman, T. David, R.Salem, R. Folman, J. Schmiedmayer: *Long-Range Order in Electronic Transport through Disordered Metal Films*, **319**, (2008), 1226.

[19] L. Della Pietra, S. Aigner, Ch. vom Hagen, S. Groth, I. Bar-Joseph, H. Lezec and J. Schmiedmayer: *Designing potentials by sculpturing wires*, Phys. Rev.A **75** 063604, (2007),.

[20] M. Wilzbach, A. Haase, M. Schwarz, D. Heine, K. Wicker, X. Liu, K.-H. Brenner, S. Groth, Th. Fernholz, B. Hessmo and J. Schmiedmayer: *Detecting Neutral Atoms on an Atom Chip*, Fortschr. Phys. **54**, (2006), 746 764.

[21] M. Wilzbach, D. Heine, S. Groth, X. Liu, B. Hessmo, J. Schmiedmayer: *A simple integrated single-atom detector*, arXiv: **0801.3255v1**, (2008).

[22] R. Folman, P. Krüger, J. Schmiedmayer, J. Denschlag and C. Henkel: *Microscopic Atom Optics: From Wires to an Atom Chip*, Advances in Atomic, Molecular, and Optical Physics VOL.**48**, (2002),.

[23] A del Campo et al: *SU-8: a photoresist for high-aspect-ratio and 3D submicron lithography*, J Micromech. Microeng. **17**, (2007), R81-R95.

Acknowledgements

Thanks to:

Jörg Schmiedmayer and Björn Hessmo: For giving me the opportunity to work in interesting and modern field of science and technology.

Dennis Heine and Thomas Raub: For patiently explaining the experiment to me.

The atom chip group: For a time of fun and for always challenging me to learn new things.

The ZMNS: For always helping me out, if some device was not working or a red light was blinking on it.

Martin Trinker: For introducing me into the clean room and teaching me literally everything I know about fabrication.

Wolfgang Rohringer, Babara Stix and Christian Koller: Wolfi for being my office neighbor for years and therefore being always my first target, if I had something to discuss. Babsi for helping me out with any theoretical problem I came up. Chrussi for discussions at every time of the day about every topic in the world.

Fachschaft Physik: For being my home for years. I have learned much more there, not only about life, but also about physics than in any lecture.

Christina Hofstätter, Florian Wippel and Leila Teymournia: For being the best learning group ever because of not wasting too much time with learning.

My family: For supporting me in every possible way.

Kathi: For the sunshine of your love.